

Organic Light Detectors: Photodiodes and Phototransistors

Kang-Jun Baeg, Maddalena Binda, Dario Natali, Mario Caironi,* and Yong-Young Noh*

While organic electronics is mostly dominated by light-emitting diodes, photovoltaic cells and transistors, optoelectronics properties peculiar to organic semiconductors make them interesting candidates for the development of innovative and disruptive applications also in the field of light signal detection. In fact, organic-based photoactive media combine effective light absorption in the region of the spectrum from ultraviolet to near-infrared with good photogeneration yield and low-temperature processability over large areas and on virtually every substrate, which might enable innovative optoelectronic systems to be targeted for instance in the field of imaging, optical communications or biomedical sensing.

In this review, after a brief resume of photogeneration basics and of devices operation mechanisms, we offer a broad overview of recent progress in the field, focusing on photodiodes and phototransistors. As to the former device category, very interesting values for figures of merit such as photoconversion efficiency, speed and minimum detectable signal level have been attained, and even though the simultaneous optimization of all these relevant parameters is demonstrated in a limited number of papers, real applications are within reach for this technology, as it is testified by the increasing number of realizations going beyond the single-device level and tackling more complex optoelectronic systems. As to phototransistors, a more recent subject of study in the framework of organic electronics, despite a broad distribution in the reported performances, best photoresponsivities outperform amorphous silicon-based devices. This suggests that organic phototransistors have a large potential to be used in a variety of optoelectronic peculiar applications, such as a photo-sensor, opto-isolator, image sensor, optically controlled phase shifter, and opto-electronic switch and memory.

1. Introduction

Organic π -conjugated small molecules and polymers are emerging materials due to their potential to realize large area and flexible optoelectronic devices^[1] by cost effective printing methods derived from graphic arts.^[2] Moreover, by controlling the molecular structure, their optoelectronic properties can be easily tuned to optimize radiative recombination, charges transport, or photogeneration depending on the targeted application. This has enabled the successful development of organic light-emitting diodes (OLEDs),^[3] organic field-effect transistors (OFETs),^[4] organic photovoltaics (OPVs),^[5,6] organic memories,^[7] and organic sensors,^[8,9] and currently a few pioneer companies are starting the commercial exploitation of this technology.

Organic semiconductors are also very appealing for light detection applications. In fact, in the region from UV to the near-infrared (NIR) the spectral sensitivity can be made panchromatic or selectively tuned to specific wavelengths. The low-temperature processability over large areas and on virtually every substrate makes it possible to target innovative applications and/or to realize original optoelectronic systems such as: large-area imagers and scanners, either flat or conformable to curved

surfaces, for visible light or for X-ray detection in biomedical applications; all-organic, short-range optoelectronic plastic-fiber based transceivers; position sensitive detectors; integrated sensoristics for Lab-on-a-chip. While traditionally representing a niche in organic electronics, it is indeed clear that organic light sensors have advantages that make them suitable for adoption in real applications.

Here, after reviewing the fundamentals of charge photogeneration in organic π -conjugated molecules in Section 2, in Section 3 we introduce the operation mechanisms of the most widely adopted architectures for organic photodetectors. Two-terminals devices, namely organic photodiodes (OPDs) and photoconductors, are dealt with in Section 3.1 and Section 3.2, respectively; three-terminal devices, namely organic phototransistors (OPTs), are presented in Section 3.3.

Section 4 is dedicated to a survey on OPDs, and is organized on the basis of the targeted region of the spectrum: photoactive materials and detectors for the visible are presented in Section 4.1.1, panchromatic and wavelength selective devices are

Prof. Y.-Y. Noh
Department of Energy and Materials Engineering
Dongguk University
26 Pil-dong, 3-ga, Jung-gu, Seoul, 100-715
Republic of Korea
E-mail: yynoh@dongguk.edu

Dr. K.-J. Baeg
Nano Carbon Materials Research Group
Korea Electrotechnology Research Institute (KERI)
12, Bulsan-ro 10beon-gil, Seongsan-gu, Changwon
Gyeongsangnam-do 642-120, Republic of Korea
Dr. M. Binda, Dr. D. Natali, Dr. M. Caironi
Center for Nano Science and Technology @PoliMi
Istituto Italiano di Tecnologia
Via Pascoli 70/3, 20133 Milano, Italy
E-mail: mario.caironi@iit.it

Dr. D. Natali
Dipartimento di Elettronica e Informazione
Politecnico di Milano
P.zza L. da Vinci, 32, 20133 Milano, Italy

DOI: 10.1002/adma.201204979



discussed in Sections 4.1.2 and 4.1.3 respectively; UV detectors are presented in Section 4.1.4. In Section 4.2 we focus on a very important aspect of OPDs, which is the reduction of dark currents in order to achieve high signal-to-noise ratios. Section 5 is dedicated to OPTs. Here the survey is divided on the basis of the adopted semiconductor, being it a small molecule^[10] (5.1) or a polymer (5.2). In the case of small molecules, particular attention is paid to the deposition process: vacuum deposited molecules are presented in Section 5.1.1, solution processed ones in Section 5.1.2. Section 5.1.3 is dedicated to single-crystal based OPTs. Finally in Section 6 an overview of the applications of organic photodetectors in advanced architectures or systems is presented, to provide the reader with the status of the progress in this field: organic-based transceivers are dealt with in Section 6.1, digital imagers in Section 6.2 and other applications, comprising position detectors and all-printed detectors, are presented in Section 6.3.

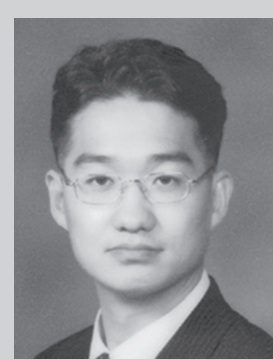
2. Charge Photogeneration

In organic semiconductors a neutral excited state termed exciton, which is a bound electron-hole (e/h) pair with a binding energy of a few hundreds of meV, is formed upon photon absorption.^[11] The *photogenerated exciton* is obviously a spinless excitation (singlet), but it is worth reminding that the relative orientation of e/h spins plays a sizeable role in organics because of the strong e/h pair correlation, so that, in addition to singlet excitons, triplet excitons can be generated as well (albeit not through photon absorption). In the following we will refer to singlet excitons unless otherwise stated.

The relatively strong exciton binding energy, which is a consequence of low dielectric constant, of electron-electron correlation and of electron-phonon coupling phenomena peculiar to π -conjugated compounds, inhibits the spontaneous dissociation of the exciton into free e/h pairs, as it occurs in inorganic semiconductors.

Before discussing how an exciton can yield free charges, we point out that photogeneration has a number of concurrent phenomena which it has to compete against, namely: *i)* radiative decay (ns time scale), *ii)* exciton diffusion, *iii)* exciton quenching. Regarding point *ii*), singlet excitons diffuse by hopping according to a generalized Förster mechanism, which involves a long-range electrostatic coupling between a starting and a final hopping site and requires spectral overlap of the emission spectrum of the former and absorption spectrum of the latter. Typical diffusion lengths are in the range of 10 nm. Regarding point *iii*), a non-exhaustive list of possible quenching paths includes: non radiative decay to ground state; intersystem crossing, which is a singlet to triplet exciton conversion; singlet-singlet (singlet-triplet) annihilation, with the generation of a ground state and of a higher excited singlet (triplet) state; singlet-charge annihilation. The interested reader is referred to Ref.^[12] and^[13] for a detailed discussion on these issues.

Firstly we briefly describe photogeneration in *pristine semiconductors*^[13] (**Figure 1**). Due to the relatively large exciton binding energy, a non-negligible potential barrier separates the excitonic state from the charge pair state. Application of an external electric field may reduce this barrier and enhance



Yong-Young Noh is Assistant Professor in the Department of Energy and Materials Engineering at Dongguk University in Seoul, Republic of Korea. He received Ph.D. in 2005 at GIST (Republic of Korea) and then worked at the Cavendish Laboratory (Cambridge, UK) as a post-doctoral associate with Prof. H. Sirringhaus from 2005 to 2007. After then he worked in ETRI (Republic of Korea) as a senior researcher from 2008 to 2009 and in Hanbat National University (Republic of Korea) as an assistant professor from 2010 to 2012. Prof. Noh has expertise in organic and printed electronics, especially printed OFETs, oxide TFTs, OPVs, and OLEDs.



Mario Caironi is a Team Leader at the Center for Nanoscience and Technology @PoliMi in Milan of the Istituto Italiano di Tecnologia. He obtained his Ph.D. in 2007 at Politecnico di Milano and then joined Prof. H. Sirringhaus' group at the Cavendish Laboratory (Cambridge, UK) to work on inkjet printed, downscaled organic field-effect transistors (OFETs), and on charges injection and transport in high mobility polymers. He is currently interested in direct-writing and roll-to-roll processes for organic optoelectronics, in the device physics of OFETs and in molecular junctions based opto-electronic devices.

photogeneration; the yield dependence on the electric field shows a threshold-like behavior. In addition to charge generation from thermalized singlet states (S_1), excess energy may be used to overcome the barrier. In the literature two models have been proposed so far. On the one hand, Pope and Geacintov focus on *photon excess energy*^[14] if a high energy singlet exciton (S_n) is generated, during its relaxation to the lowest singlet state (S_1) branching to the charge pair state may occur. This process, also known as autoionization, competes with singlet relaxation and has to occur on a very short (<100 fs) time scale. On the other hand, according to Arkhipov and co-workers, vibrationally hot singlet S_1 states (generated upon exciton annihilation processes or due to S_n to S_1 decaying processes) may take advantage of their *excess vibrational energy* to split into charges.^[15] Due to the competition with S_1 cooling, this mechanism has a strong time-dependent nature.

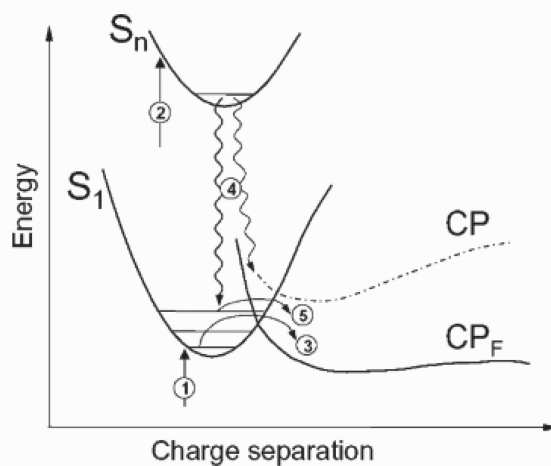


Figure 1. Charge pair generation model in pristine materials. S_1 and S_n are the lowest and a high energy singlet exciton. CP is the charge pair state, and CP_F is the CP state modified by the applied electric field lowering the barrier for exciton breaking. Process 1(2) optically generates $S_1(S_n)$; process 3 represents charge generation starting from a thermalized S_1 state; process 4 is relaxation from S_n to S_1 , which may branch to give a charge pair (autoionization) or results in the population of vibrationally hot S_1 states, which then can overcome the barrier resulting in charge pairs (process 5, Ref. [15]). Reproduced with permission from Ref. [13], Copyright 2007 American Chemical Society.

Some pristine materials (e.g., polythiophene derivatives) show sizeable charge pair production even in the absence of electric field or excess energy: it has been suggested that due to strong intermolecular interactions, sites with very low energy barriers toward charge separation may exist. At those sites, exciton breaking into charge pairs occurs almost barrier-less, and charge generation yield is primarily ruled by exciton migration to such dissociation sites.^[13]

To summarize, photogeneration in pristine organic semiconductors can be from poorly to mildly efficient (pristine single-crystals representing an exception thanks to their high degree of order^[16]), but most importantly rather impractical, as it is strongly dependent on the availability of excess energy, which can come from the electric field, from optical excitations or can have thermal origin.

To enhance photogeneration yield it is common to exploit the phenomenon of *photoinduced charge separation* occurring at so called Donor (D) - Acceptor (A) interfaces (Figure 2). We term Donors (Acceptors) molecules that are characterized by a low ionization potential (high electron affinity). Upon photoexcitation of D (or of A), an exciton reaching a D/A interface decays into a charge transfer (CT) state, with the electron residing on the lowest unoccupied molecular orbital (LUMO) of A and the hole residing on the highest occupied molecular orbital (HOMO) of D (provided that the CT state represents the lowest energy configuration).^[17] This process turns out to occur on a sub-100 fs time scale thus being very competitive with respect to other exciton deactivation paths. In the framework of photogeneration, the advantage of CT states is that e/h pairs are less coulombically bound and hence more prone to dissociation.

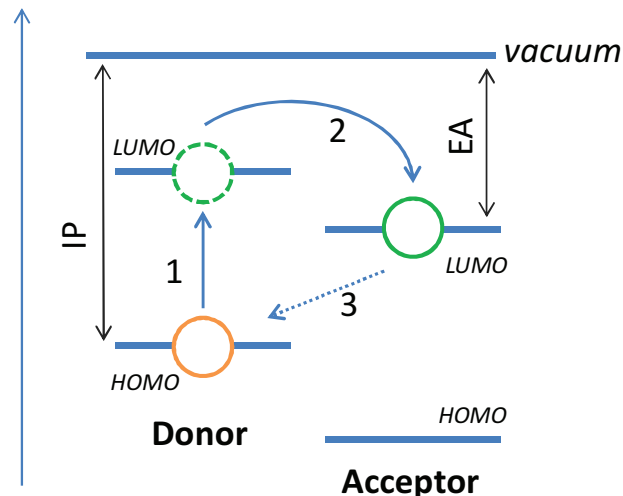


Figure 2. Simplified picture of a D/A interface drawn assuming vacuum level alignment. Process 1 refers to exciton generation upon photon absorption in the donor; process 2 refers to ultrafast charge separation at the interface; process 3 to the usually scarcely effective recombination between the electron on the acceptor and the hole on the donor. Also shown are the ionization potential of the donor (IP) and the electron affinity of the acceptor (EA).

High photogeneration yields require that the generation of excitons occurs within a diffusion length from a D/A interface, thus suggesting the importance of a high degree of intermixing between D and A phases. On the other hand, it must be taken into account that after generation holes (electrons) have to be collected, which requires the continuity of D (A) phases, thus suggesting that a certain degree of demixing between D and A is mandatory to avoid dead-end transport paths and to ensure effective charge collection. From a device point of view, various solutions have been adopted, from bi- (or multi-) D/A layers^[18,19] to bulk heterojunction.^[20,21] In the latter case the D/A blend nano-morphology has a critical impact on device performances.

Photogeneration at D/A interfaces is expected to be effective for both singlet and triplet excitons^[22] (provided that the exchange interaction is small compared to the Coulomb attraction of the CT state). It is worth noting that on the one hand a triplet has a longer lifetime than a singlet exciton (μ s or ms versus ns time scale), but on the other hand a triplet diffuses more slowly than a singlet, because hops are restricted to adjacent sites, relying upon a short-range electron exchange (Dexter-type) mechanism requiring spatial overlap of the wavefunctions of the starting and target sites.^[23] Hence the triplet vs. singlet diffusion length is difficult to predict and it is strongly material dependent.

Going beyond the very simplified description given so far for D/A interfaces and related phenomena is outside the scope of this paper, nevertheless it is worth making the reader aware of implicit approximations done and giving a brief account of open issues in this field.

A first *caveat* must be given on the energetic levels at a D/A interface, which may differ from those in the bulk of pure D or A phases. In fact interface dipoles, resulting in a shift of energetic levels at the interface, may arise because of: (eventually

partial) ground state CT (due to weak van der Waals dispersion forces, electrostatic interactions, steric repulsions); polarization effects (due to reorganization of the electronic density within the molecules). These phenomena are very sensitive to the spatial and mutual nanoscale arrangement of molecules at the interface, and the interested reader is referred to Ref. [22] for more details.

In addition, no clear consensus on the main mechanisms ruling free charge generation at D/A interfaces has been reached yet. Firstly, it has to be pointed out that still in the CT state electron and hole are subject to their mutual coulombic attraction: with an e/h separation of 1 nm and with a relative dielectric constant $\epsilon_r = 3\text{--}4$, the binding energy is still in the range of few tenths of eV thus having a negligible probability of thermal dissociation.^[24]

Two scenarios have been proposed to explain the experimental evidence that free charge generation occurs in a very effective way at D/A interfaces. In the first one, the starting point is an already thermalized CT state. Factors which can modify the CT binding energy are:^[24] *i)* dipoles or multipoles at the interface; *ii)* entropy; *iii)* disorder; *iv)* external electric fields. Regarding point *i*), it has been shown that the binding energy of the CT state may be lowered by interaction with interface dipoles or multipoles (arising from ground state CT at the interface), provided that suitable mutual orientation of D and A molecule occurs at the interface.^[25,26] Regarding point *ii*), entropy may contribute to charge separation efficiency, as more and more sites are increasingly available upon increasing the e/h mutual distance.^[27] Regarding point *iii*), thanks to energetic disorder it is likely to find neutral molecules adjacent to the site where the CT state resides which are energetically favorable to charge separation. In the second scenario, an exciton facing a D/A interface couples to hot CT_n states, which are more spatially extended than CT₁.^[28] Hence, the electron and the hole are more distant and their binding energy is lower than in CT₁. Effective dissociation of CT_n into free carriers can occur if the time scale for charge separation is shorter than the time scale for CT_n thermalization to CT₁.^[29] To profit from this mechanism, CT_n with large excess energy should be created. To this extent, the energy difference between the LUMO (HOMO) levels of A (D) and D (A) moieties should be maximized. Increasing the D/A LUMO (HOMO) offset can have negative impact in case of solar cells, because on the one hand the short circuit current may improve, but the open circuit voltage (which is related to energy difference between the HOMO of D and the LUMO of A) may become lower.^[24] But in the case of photodetectors, where the focus is on current signal rather than

on power delivery, this strategy could be pursued with no negative effects (at least until the so called Marcus inverted regime is not reached).^[22,30]

Finally, it is worth reminding that the generation of free e/h pair from CT state has to compete against other CT deactivation paths such as: electron (hole) back transfer to D (A) molecule thus regenerating an exciton on D(A) moiety, radiative or non radiative recombination to ground state (also termed geminate recombination).^[24] As to this latter, a possible strategy to lower the effectiveness of geminate recombination is to provide an as large as possible energetic offset between the LUMO of A and the HOMO of D, thus forcing the process in the Marcus inverted regime (as it is known to occur for instance in the case of perylenetetracarboxydiimide/ metal-free phthalocyanine and pentacene/C₆₀).^[22,31]

3. Operation Mechanisms

Generally speaking, light signal detectors convert a photon flux into a flux of charge carriers. With respect to solar cells, the target of these devices is the delivery of a photocurrent signal, rather than the delivery of electric power to a load. As a consequence, it is possible to apply an external voltage to enhance the electric field and improve carrier photogeneration and/or collection. The figures of merit are, in addition to the External Quantum Efficiency (EQE), the operation bandwidth (BW) and the signal to noise ratio (SNR). Alternatively to EQE, it is not uncommon to find Responsivity (R), which can be expressed as $R = \text{EQE} \cdot \lambda q/hc$, where λ is the wavelength of interest, h the Planck constant, c the speed of light, q the electron charge. Photodetectors can be roughly divided in three sub-categories: photodiodes, photoconductors, and phototransistors.

Photodiodes (Section 3.1) and **photoconductors** (Section 3.2) are two terminal devices where the photoactive medium is contacted by two metal contacts (Figure 3 and Figure 4). The most common topology is the vertical (sandwich-like) one, which is very similar to OPVs, but is optimized to work with a reverse applied field, with low dark-currents and to provide a fast collection of charges. Less popular is the lateral topology, which on the one hand offers direct access to the photoactive medium thus enabling direct investigations on working devices,^[32] but on the other hand is usually characterized by larger interelectrode spacings (from few to tens of micrometers, to be compared to the few hundreds of nanometers commonly adopted in vertical topology) and hence lower operation bandwidth. In photodiodes an absorbed photon can generate at best one

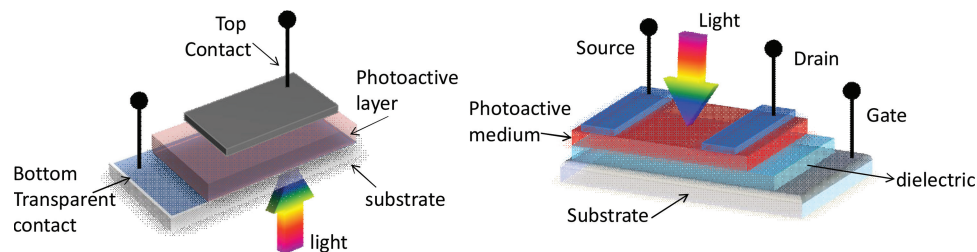


Figure 3. Typical device configurations of photodetectors. On the left a photodiode with vertical topology is shown, with the light window entrance on the bottom. On the right the typical structure of an organic phototransistor is sketched (bottom-gate/bottom-contact with top-light illumination).

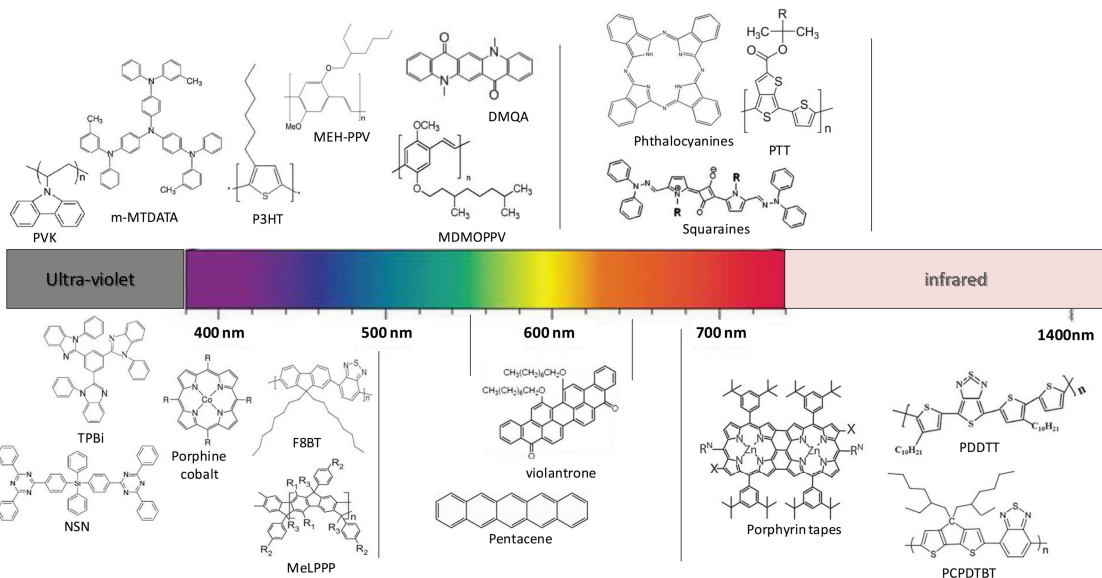


Figure 4. Some of the most widely adopted π -conjugated molecules from the UV to the NIR range of the spectrum.

electron-hole pair, therefore EQE cannot be higher than 100%: in order for this to occur, non-injecting metal-semiconductor contacts are required. In photoconductors instead, EQE can be in excess of 100%, and for this to occur contacts have to be injecting for at least one kind of carriers.^[33]

Phototransistors (Section 3.3) basically have the same three terminal configuration of OFETs (Figure 3), where three electrodes, referred to as the source, drain, and gate, are present. While in the operational mode of normal OFET the amount of current flowing (the drain current, I_d) in the accumulated channel is controlled by the magnitude of gate voltage (V_g) at a given source to drain bias (V_d),^[34] for OPTs the control of channel conductance can be additionally enabled by absorption of light.

3.1. Photodiodes

The behavior of a photodiode changes accordingly to the fate of photogenerated carriers. In fact they can be: *i*) collected at electrodes (holes at the anode and electrons at the cathode) or *ii*) can undergo recombination before collection. For case *i*) to occur, the lifetime of carriers τ must exceed the time required for them to reach the electrodes, viz. $L/\mu E > \tau$, where L is the interelectrode spacing, E the electric field and μ the charge mobility. In the following we consider the two cases separately.

Let's focus on case *i*). For the sake of simplicity we introduce the net volume photogeneration rate G , which takes into account photon absorption and dissociation efficiency. If holes and electrons have comparable mobilities, then they are extracted at the same rate from cathode and anode and charge neutrality of the active layer is ensured. This means that the electric field profile under illumination will not differ from the one in dark conditions. The photocurrent is $J = qGL$, where q is the elementary charge. The photodiode is working at its highest efficiency, as from each photogenerated pair an e^-/h^+ couple is

collected in the outer circuit. The device BW is related to the reciprocal of the carrier transit time, hence it is proportional to $\mu V/L^2$.

If mobilities are unbalanced, for instance electron mobility (μ_n) is far larger than hole mobility (μ_p), then when a photon flux starts impinging on the device, holes will tend to accumulate in the device and a positive net space charge will be established. This charge reshapes the electric field to enhance (slow down) the collection of holes (electrons) and a regime condition will be reached when holes and electrons are extracted at the same rate from the device: this implies that the externally applied voltage V has to drop almost entirely close to the anode across a region of length L' , while in the remnant $L - L'$ part of the device no net photogeneration nearly occurs due to recombination.^[35] Therefore, unbalanced mobilities result in a loss of photoactive area.^[32] To calculate L' in a one-dimensional framework, one has to consider that holes in the L' area of the semiconductor are in complete induction with negative charges on the anode, thus giving rise to a capacitance $C = \epsilon/L'$: this means that the total amount of positive charge Q_p is electrostatically upper bounded by $Q_p = CV$. As a consequence, the photocurrent will be space charge limited (SCL),^[36] following the equation $J \propto \epsilon \mu_p V^2 / L^3$. By equating the volume photogeneration rate qGL to the SCL photocurrent, an expression for L' can be obtained: $L' \propto (\epsilon \mu_p / qG)^{0.25} V^{0.5}$ and $J \propto q (\epsilon \mu_p / q)^{0.25} G^{0.75} V^{0.5}$. If G is made larger, then charge density tends to rise, but to cope with electrostatics the system has to enhance the capacitance by shrinking L' . The net result of this adaptation of the active volume to the generation rate is a sublinear dependence of J upon G and V . This regime is known as *space charge limited photocurrent*.^[37,38] It has to be noted that the actual dependence of the photocurrent can be more complicated due to mobility dependence on charge density and on the longitudinal electric field.

We now turn to the case *ii*), which is the recombination limited regime. It has first to be noted that in the field of organic

semiconductors no clear consensus has been reached yet regarding the most effective recombination mechanisms for excess carriers. Besides Langevin-type bimolecular recombination, modeling the annihilation of e^-/h^+ pairs driven by their mutual Coulombic attraction (which cannot be overwhelmed by thermally driven diffusion once the carriers are closer than the capture radius, about 20 nm at 300 K), other trap-mediated monomolecular mechanisms are gaining consensus. The interested reader is referred to Refs. [39–41] for more detailed discussions on this topic. In this context we limit ourselves to describe a simplified case, assuming that electrons (holes) are characterized by a lifetime τ_n (τ_p) due to the dominant recombination mechanism, and that, apart from carriers photogenerated close to the contacts, carriers experience recombination before collection, viz. for both electrons and holes $L/(\mu E) > \tau$.

To fix ideas we consider $\mu_n \tau_n \gg \mu_p \tau_p$ (the latter quantities are termed mobility-lifetime products). Approximately the externally applied voltage drops entirely close to the anode over a region of length L' to enhance holes collection. The extent of this region can be calculated as it follows: the time needed for a hole generated in L' to reach the anode has to be at most equal to its lifetime, viz. $\mu_p E \tau_p = L'$. Since $E \approx V/L'$, then $L' = (\mu_p \tau_p V)^{0.5}$. Finally the current is expressed as $J = qGL' = qG(\mu_p \tau_p)^{0.5}V^{0.5}$, hence it is linear on the photogeneration rate but sublinear on the applied voltage. If a sufficiently large voltage is applied, then collection occurs before recombination, L' tends to L and the photocurrent tends to saturate to qGL .

Since in the recombination limited regime an unbalanced charge region exists close to the anode, and since the larger is G , the larger is this excess charge, at very high G the device might enter into the SCL regime, where $J \propto (e\mu_p/q)^{0.25} G^{0.75} V^{0.5}$. It is worth noting that the occurrence of the SCL regime can be determined by looking at the photocurrent dependence on G , whereas the dependence on V does not give clues to discriminate between the two regimes.

If the mobility-lifetime products are the same for holes and electrons then the photocurrent can be written as $J = qG\mu\tau V/L$ for low voltages and saturates to qGL for larger voltages, and no sublinear dependence on V occurs.^[37]

As highlighted before, this simplified treatment does not take into account that mobility is usually charge density and field dependent, and that the lifetime as well might depend on the recombination center occupancy, hence the photocurrent functional dependence on V and G could be more complicated.

3.2. Photoconductors

Even if it is not the focus of this review, we give a very brief account of the working principle of photoconductors. We consider a simple case, where deeply trapped holes are substantially immobile and contacts are ohmic for electrons (the interested reader can find more cases discussed in Ref.^[33]). Contact ohmicity implies that charge neutrality is ensured in the device, hence for every collected electron another one will be injected, until an electron/hole recombination event occurs. Since more than one electron can flow in consequence of a single absorbed photon, an efficiency higher than 100% is possible, according to the ratio between the electron/hole

recombination time τ and the electron transit time, which is termed *photoconductive gain*. In this regime the photocurrent follows the expression $J = qGL[\tau/(L^2/\mu V)]$. It is worth noting that the device BW is proportional to the reciprocal of τ and it is independent on the carrier transit time, hence a tradeoff exists between the photoconductive gain and the BW. For a photoconductor model taking into account the hopping nature of transport thus including the effect of the mobility dependence on charge density, the interested reader is referred to Ref. [42].

3.3. Phototransistors

Two different effects typically occur in active channel layers as the result of illumination for OPTs:^[43,44] when the transistor operates in accumulation ($V_g < V_{Th}$ for a p-channel device, where V_{Th} represents the threshold voltage), the so-called photovoltaic effect is dominant, whereas when the device operates in the depletion ($V_g > V_{Th}$), I_d increases with optical power due to a photoconductive effect.

3.3.1. OPT Photovoltaic Mode

In photovoltaic mode, illumination results in a photo-induced shift of V_{Th} towards more positive (negative) values for p-channel (*n*-channel) devices. If we consider the case of a p-channel OPT, when absorption occurs, the photo-generated holes easily flow to the drain electrode whereas electrons accumulate under the source electrode, where they effectively lower the holes injection barrier between the source and the semiconductor channel. The accumulated negative carriers can effectively reduce the injection barrier of holes at the source electrode. The lowered injection barrier induced by light irradiation results in an effective decrease in contact resistance and in a positive shift of V_{Th} , and thereby in a significant increase in I_d .^[45–47] Moreover, photogenerated electrons can also be trapped at the semiconductor/dielectric interface by electron-capturing moieties, such as hydroxyl groups on SiO_2 dielectric layer or other sources. The photocurrent caused by the photovoltaic effect can be expressed as Equation (1):^[45,46]

$$I_{ph,pv} = g_m \Delta V_{Th} = \frac{AkT}{q} \ln \left(1 + \frac{\eta q \lambda P_{opt}}{I_{pd} hc} \right) \quad (1)$$

where η is the photogeneration quantum efficiency, P_{opt} the incident optical power, I_{pd} the dark current for minority charges, hc/λ the photon energy, g_m the transconductance, ΔV_{Th} the threshold voltage shift, and A a proportionality parameter.^[48]

3.3.2. OPT Photoconductive Mode

When the device is in the off state ($V_g > V_{Th}$ for *p*-channel), photo-generated I_d shows a linear increase with optical power due to a photoconductive effect. The situation is similar to two-terminal devices discussed in Section 3.2, but with the additional gate terminal responsible for a transverse electric field enhancing photogeneration. The current can be modeled according to Eq. (2):^[49]

$$I_{\text{ph},\text{pc}} = (q \mu_p p E) WD = B P_{\text{opt}} \quad (2)$$

where μ_p is the mobility of majority charge carriers, p the charge concentration, E the electric field in the channel, W the gate width, D the depth of absorption region, and B a proportionality factor.

In addition to the fundamental OFET characteristics, such as the field-effect mobility (μ_{FET}), the V_{Th} , the subthreshold swing (SS), the figures of merit specific to OPTs are responsivity (R) and photocurrent on/off ratio. The device R can be defined with the following equation:

$$R = E Q E \frac{\lambda q}{hc} = \frac{I_{\text{ph}}}{P_{\text{opt}}} = \frac{I_{\text{d,ph}} - I_{\text{d,dark}}}{P_{\text{opt}}} \quad (3)$$

where, I_{ph} is the source-drain photocurrent, P_{opt} the incident optical power, $I_{\text{d,ph}}$ and $I_{\text{d,dark}}$ are the drain current in dark and under illumination, respectively.

4. Photodiodes

4.1. Photoactive Materials and Detectors for Different Spectral Regions

Here we will review photodiodes/photoconductors for different spectral regions, ranging from UV to near infra-red (NIR) light. There is a rising interest also for adopting organic photodiodes in the field of radiation detection, mainly direct and indirect X-ray detection and alpha particle detection. The interested reader is referred to recent reviews and papers specific to the field.^[50–53]

4.1.1. Visible Photodetectors

Based on the typical size of their optical energy bandgap, organic semiconductors find natural and profitable exploitation as active materials in devices operating in the visible. First examples were demonstrated by different groups^[18,54–56] between 1990 and 2000. Since then, many successful realizations of OPDs have been reported covering with remarkable efficiency the whole visible spectrum. Either exploiting small molecules or polymer compounds, most of them are based on heterojunction D/A systems. In the case of small molecules, where molecular beam deposition techniques enable higher degree of control over the active material nanostructure and morphology, extremely fast and efficient visible-sensitive photodiodes, with EQE as high as 75% and BW up to 430 MHz, were reported by the group of Forrest already in 2000.^[57] More complicated is the case of solution processed devices, where the heterojunction morphology at the nanoscale is poorly controllable and selection of D/A couples with suitable mixing tendency plays a key role. However, for the well-known and thoroughly studied solution processed poly(3-hexylthiophene) (P3HT)-phenyl-C₆₁-butyric acid methyl ester (PC₆₁BM) D/A couple, which is characterized by broad absorption and relatively high carriers mobility, good coverage of the range between 400 and 600 nm with peak EQE above 70% has been reported by

many groups.^[58–60] Poly(phenylene-vinylene) derivatives like poly[2-methoxy-5-(2-ethylhexyloxy)-1,4-phenylene-vinylene] (MEH-PPV) or poly(2-methoxy-5-(3'-7'-dimethyloctyloxy)-1,4-phenylenevinylene) (MDMO-PPV) form with PC₆₁BM another very well known D/A couple, with which high EQE (around 60%) is achieved for blue-green light detection up to about 550 nm.^[61–64] Higher analogues of PC₆₁BM like PC₇₁BM, having extended optical absorption in the visible, have also been proposed in the literature.^[65] Recently new classes of materials have emerged as promising donors or acceptors, such as polyfluorene derivatives and copolymers^[66]. Examples have been reported of all-polymeric OPDs reaching 26% EQE based on poly([9,9-diptylfluorene]-2,7-diyl-alt-[4,7-bis(3-hexylthien-5-yl)-2,1,3-benzothiadiazole]-2,2-diyl) (F8TBT) acceptor in blend with P3HT.^[67,68] Good results have been also demonstrated for polyfluorene copolymer 9,9'-diptylfluorene-co-benzothiadiazole (F8BT) acting as the donor in bulk-heterojunction with perylene diimides (PDI).^[69] In this realization, PDI molecules are presented as promising acceptor materials in alternative to fullerenes due to their very high electron affinity, good electron mobility and solubility. Although still not comparable to the performance of P3HT:PC₆₁BM, OPDs based on F8BT:PDI blend achieved a reasonable EQE of about 15% over the 400–525 nm range.

Compared to blue-green light detection, much fewer examples are reported in the literature for the case of red-light sensitive OPDs, this mainly due to small bandgap compounds being typically prone to issues regarding their synthetic accessibility, chemical stability and solubility.^[70,71] Moreover, as the energy gap is decreased, finding molecular D/A combinations with suitable energy alignments becomes increasingly difficult. Nevertheless, the existence of many applications based on red-NIR light detection, e.g. in the fields of optical communications,^[72,73] remote control, environmental control or biomedicine,^[74] has recently pushed a lot the development of such kind of devices.^[75–78] On the side of small molecules, phthalocyanines definitely represent the most classical choice for red photons harvesting thanks to their typical absorption peaked in the 600–700 nm range. Either exploited in their unsubstituted and substantially insoluble form^[79] deposited by thermal evaporation, or in their substituted soluble forms, they have enabled very good performance in the NIR. Campbell et al.^[80] reported a photoconductor based on soluble octabutoxy tin naphthalocyanine dichloride (OSnNcCl₂) as the pristine active material. For this device, photoconductive gain of 10 at 1000 nm was demonstrated. Another extremely interesting class of low bandgap molecules is based on squaraine compounds, that are characterized by chemical and photochemical robustness and whose absorption band is typically located between 600 and 800 nm. For instance, they have been recently employed^[81,82] in blend with PC₆₁BM to develop a photodiode with peak EQE of about the 15% in the 700–800 nm range. Finally, square planar metal bis-dithiolenes^[83] can be rationally tuned as effective light harvesters between 700 and 1600 nm. It has been recently shown that responsivity limitations encountered in the first realizations,^[84–86] can be overcome by means of a peculiar metal/semiconductor/insulator/metal sandwich structure, which, although unsuited to steady state detection, results in responsivities to periodic light signal larger than

0.2 A/W (up to 1.2 A/W upon blending with carbon black) with a bandwidth up to 1 MHz.^[87]

In the case of polymers, which typically show broader absorption compared to small molecules (albeit with some exceptions^[88]), lowering the bandgap to cover the red region of the spectrum eventually results in OPDs with broadband spectral operation, sometimes extended even into the first region of the near-infrared (~700–1500 nm), as discussed more in detail in Section 4.1.2. In many applications, in spite of a broadband response, a wavelength selective responsivity is a premium feature. Notable realizations are discussed in Section 4.1.3.

4.1.2. Panchromatic Photodetectors

Strongly pushed by research on organic photovoltaics, where broadband harvesting of the solar spectrum is a key requirement to enhance the efficiency of solar cells, the development of panchromatic active materials can also be of high interest for OPD devices in some fields of applications, like optical remote sensing for reconstruction of morphological profiles,^[89] environmental control^[90] or laboratory instrumentation for optical spectroscopy.

In the case of conjugated polymers, very low bandgaps can be obtained by exploiting a well-known strategy based on polymerization of fused heterocyclic rings. In 2007, the group of Yang^[91] demonstrated a photodetector with responsivity extended up to 900 nm (EQE ~ 40% at 800 nm) based on the bulk-heterojunction of a suitably designed ester group modified polythieno[3,4-*b*]thiophene (PTT) polymer with PC₆₁BM. A similar approach was adopted by Gong et al.^[92] to develop a panchromatic detector with photoresponsivity ranging from 300 to 1450 nm (EQE ~ 30% at 900 nm), based on the low bandgap poly(5,7-bis(4-decanyl-2-thienyl)-thieno(3,4-*b*)diathiazole-thiophene-2,5) (PDDTT) polymer again blended with PC₆₁BM. Good photoresponse at long wavelengths up to about 850 nm was also demonstrated for the D/A couple based on the low bandgap copolymer poly[2,6-(4,4-bis(2-ethylhexyl)-4H-cyclopenta[2,1-*b*;3,4-*b*']dithiophene)-alt-4,7-(2,1,3-benzothiadiazole)] (PCPDTBT) in blend with PC₇₀BM, widely exploited in the field of organic photovoltaics to enhance the harvesting of solar irradiation in the NIR range.^[93,94]

On the side of small molecules, porphyrin-based compounds represent a promising class of materials where π -conjugation can be extended to address long wavelengths absorption. Recently, solution processed conjugated porphyrin arrays, where porphyrin units are connected one to the other in a tape-like shape, have been exploited^[95,96] to achieve 10% EQE at 1400 nm in bilayer detectors with thermally evaporated C₆₀ as the electron acceptor. Fundamental to this achievement was the exploitation of suitable additives blended with the donor material, capable of improving short-range ordering and electronic coupling between adjacent tapes thus further red-shifting the device photoresponse. A BW wider than 50 MHz was also demonstrated for these OPDs.

Alternatively, extended photoresponse in the NIR is often achieved by exploiting hybrid systems where organic small molecules and polymers are used in combination with nanostructured organic or inorganic materials. This is the case of the photodetectors proposed in 2009 by Arnold et al.,^[97] where

excitons generated on semiconducting Carbon NanoTubes (CNTs) are dissociated at the interface with a C₆₀ layer. Conjugated polymers (either MDMO-PPV or P3HT) wrapped around the CNTs are used to achieve good solubility, provide isolation between different nanotubes and help the uniformity of the deposited film. High polydispersity of CNTs diameters enable broad spectral coverage from 400 to 1600 nm to be achieved. Low bandgap semiconductors based on inorganic NanoCrystals (NCs), like PbSe or PbS, have been exploited as well by many groups^[98–102] to address light detection at wavelengths longer than 1 μ m. Recently, a NIR lateral photoconductor based on PbS NCs-PC₆₀BM D/A bilayer was presented^[103] where the performance of the device in terms of quantum efficiency and response speed is tuned by fine engineering of the NCs-organic hetero-interface. Hybrid inorganic/organic ternary blends have been recently proposed where small bandgap NCs, like PbS NCs, are used in combination with organic D/A couples, e.g. P3HT:PC₆₁BM, in order to boost the responsivity in the IR. Enhancement of photoresponsivity with respect to binary NCs/organic blends has been attributed to double charge transfer of both the photoexcited hole and electron from the NC respectively towards the donor and the acceptor phase in the organic blend, exploiting the better charge transport of organic phases with respect to NCs network.^[104,105]

The reader is referred to Table 1 for a collection of features and performance related to many organic and hybrid realizations for visible and NIR photodetectors.

4.1.3. Wavelength Selective OPDs

The *selective* approach exploits the natural selectivity of organic semiconductors absorption arising as a consequence of weak inter-molecular interaction in the solid-state. This peculiarity suggests the useful application of organic photodetectors in different fields: full-color digital camera or camcorder image sensor arrays, where light-wasting color filtering traditionally used in Si-based technology could be avoided; artificial systems mimicking human eyes;^[106] industrial colorimetric measurements;^[107,108] spectral biological imaging.^[60] For many of these applications, tunability of the spectral response is of fundamental interest. For instance, a system was proposed^[108] in 2007 where the functionality of a three-stimuli^[109] color-sensor was reproduced by combining signals from three organic photodiodes with suitable spectral response. In particular, three different organic semiconductors, namely methyl-substituted ladder-type *para*-polyphenylene (MeLPPP), regioregular P3HT and violanthrone 16,17-bis(octyloxy)anthrax[9,1,2-cde]-benzo[rst]pentaphene-5,10-dione, were carefully selected in order to develop three photodiodes with photocurrent action spectra strictly resembling the color matching functions of the standard observer CIE1931. A similar approach was exploited also by another group^[110] to realize a stacked structure composed of three organic photodetectors individually sensitive to one of the three primary colors. Thermally evaporated tetra(4-methoxyphenyl) porphirine cobalt complex (CoTPP), NN'-dimethylquinacridone (NN'QA) and zinc phthalocyanine (ZnPc) were chosen as blue, green and red sensitive photoactive materials respectively. Each photodiode was built on an individual glass substrate, had ITO (Indium Tin Oxide) as both

Table 1. Visible-NIR Photodetectors based on organic semiconductors or hybrid materials.

Method	Active material Device structure ^{a)}	Spectral window	Responsivity @V _{BIAS} (Light source, Intensity)	I _{dark} (V _{BIAS})	Bandwidth (t_R) ^{b)}	Ref.
Vacuum	CuPc/A1 ^{c)} multilayer alternated sandwich-like	525–725 nm	390 mA/W @ -10 V (650 nm, <3 mW/cm ²)	NA	430 MHz (720 ps)	[57]
	Pentacene/C60 multilayer alternated sandwich-like	450–690 nm	524 mA/W @ -3.5 V (660 nm, 1.54 mW/cm ²)	0.2 mA/cm ² (-3.5 V)	NA	[200]
	CuPc/A2 ^{d)} Bilayer sandwich-like	450–750 nm	30 mA/W @ -3V (525 nm, NA) 20mA/W @ -3V (625 nm, NA)	1 mA/cm ² (-7 V)	70 MHz (~40 ns)	[72]
	Pentacene/C60 Bilayer sandwich-like	500–690 nm	112 mA/W @ -10 V (580 nm, NA) 56 mA/W @ -10V (690 nm, NA)	NA	80 MHz	[201]
	CoTPP/Alq3 Bilayer sandwich-like	~400–460 nm	27 mA/W @ >10V (70 V) (425 nm, 50 mW/cm ²)	NA	NA	[110]
	NN'QA/Alq3 Bilayer sandwich-like	450–550 nm	25 mA/W @ ~10 V (500 nm, 50 mW/cm ²)	NA	NA	
	ZcPc/Alq3 Bilayer sandwich-like	550–750 nm	22 mA/W @ ~10 V (600 nm, 50 mW/cm ²)	NA	>2 kHz	
Solution/ vacuum	CuPc (a)/F16CuPc (b) Three layers: (a)/(a):(b)/(b) sandwich-like	550–700 nm 750–850 nm	~60 mA/W @ -9 V (808 nm, 3 mW/cm ²)	1 μA/cm ² (-10 V)	14 MHz (80 ns)	[79]
	OSnNcCl ₂ sandwich-like	400–600 nm 800–1100 nm	Photoconductive gain ~15 @ -8 V (1064 nm, NA)	NA	< 3 kHz	[80]
	Zn-metallated porphyrin/C60 Bilayer sandwich-like	<1350 nm	~70 mA/W @ 0V (1345 nm, ~1 mW/cm ²)	NA	56 MHz (~2 ns)	[95]
	Zn-metallated porphyrin:PC ₆₁ BM:pyridine BHJ/C60 Bilayer sandwich-like	<1600 nm	119 mA/W @ 0V (1400 nm, NA)	NA	NA	[96]
	MDMO-PPV:_CNT/C60 sandwich-like	400–1450 nm	23 mA/W @ -0.7 V (1155 nm, NA)	NA	31 MHz (~7 ns)	[97]
	P3HT:PC ₆₁ BM BHJ sandwich-like	400–600 nm	339 mA/W @ 0 V (600 nm, NA)	NA	NA	[60]
	P3HT:PC ₆₁ BM BHJ sandwich-like	400–650 nm	100mA/W @ -1 V (468 nm, 40 mW/cm ²)	<10 nA/cm ² (-1 V)	62 kHz	[58]
Solution	P3HT:PC ₆₁ BM BHJ sandwich-like	350–625 nm	177 mA/W @ -1 V (550 nm, NA)	~100 nA/cm ² (-1 V)	500 kHz	[202]
	P3HT:PC ₆₁ BM BHJ sandwich-like	400–600 nm	390 mA/W @ -5 V (540 nm, NA)	65 nA/cm ² (-5 V)	100 kHz	[59]
	P3HT:PC ₆₁ BM BHJ sandwich-like	400–600 nm	240 mA/W @ -5 V (532 nm, 191 μW/cm ²)	~ μA/cm ² (-5 V)	1 MHz (~ 40 ns)	[185]
	MEH-PPV:PC ₆₁ BM BHJ sandwich-like	350–550 nm	140 mA/W @ -4 V (488 nm, ~1 μW/cm ²)	<1 nA/cm ² (-4 V)	(~ ms)	[61]
	Polyfluorene F8T2:PC ₆₁ BM BHJ sandwich-like	~400–500 nm	~670mA/W @ -10 V (460 nm, 9mW/cm ²)	~1 mA/cm ² (-10 V)	~50 MHz	[66]
	F8BT:PDI BHJ sandwich-like	400–600 nm	~40 mA/W @ -0.5 V (530 nm, NA)	~8 nA/cm ² (-0.5 V) with EBL	NA	[69]
	P3HT:F8TBT BHJ sandwich-like	400–600 nm	~100 mA/W @ -0.5 V (500 nm, NA)	4 nA/cm ² (-0.5 V) with EBL	NA	[67]
	PDDTT:PC ₆₁ BM BHJ sandwich-like	~300–1400 nm	170 mA/W @ -0.5 V (800 nm, 0.22 mW/cm ²)	<nA/cm ² (-1 V) with EBL + HBL	NA	[92]
	PCPDTBT:PC ₇₁ BM BHJ sandwich-like	~300–900 nm	~300 mA/W @ 0 V (800 nm, 80 mW/cm ⁻²)	NA	NA	[94]
	PTT:PC ₆₁ BM BHJ sandwich-like	~300–950 nm	267 mA/W @ -5 V (800 nm, NA)	~100 μA/cm ² (-1 V)	4 MHz	[91]
Solution/ Hybrid	Squaraine:PC ₆₁ BM BHJ sandwich-like	650–850 nm	85 mA/W @ -1 V (700 nm, ~10 mW/cm ²)	2 nA/cm ² (-1 V) with EBL	1 MHz	[82]
	CdSe QDs/spiro-TPD Bilayer lateral	350–600 nm	Photoconductive 410 mA/W @ -300 V (400 nm, NA) ~61 mA/W @ -300 V (590 nm, NA)	~100 mA/cm ² (-100 V)	NA	[203]
	PbS QDs:P3HT:PC ₆₁ BM BHJ sandwich-like	400–1450 nm	160 mA/W @ -5V (1220 nm, NA)	~4 μA/cm ² (-5 V)	2.5 kHz	[104]

^{a)}In case of bi- or multilayers active materials are separated by a slash, whereas in case of bulk heterojunction active materials are separated by a colon; ^{b)} t_R is the response time; ^{c)}A1: 3,4,9,10-perylenetetracarboxylic bis-benzimidazole (PTCBI); ^{d)}A2: N,N'-bis(2,5-di-tert-butylphenyl)3,4,9,10-perylenedicarboximide (BPPC).

the bottom and the top electrode, and was provided with an extra tris-8-hydroxyquinoline aluminum (Alq_3) layer acting as electron acceptor/transporter thus improving the EQE (ranging from 5% to 8% for the different detectors at their peak wavelength). Despite the spectral selectivity of the individual photodiodes being not excellent, good overall color separation for the color sensor was achieved by stacking the detectors in the order of blue, green, and red from top to bottom. Another recent paper^[111] exploits a similar stacking approach in order to enhance the spectral selectivity of red-sensitive OPDs based on copper phthalocyanine-C₆₀ heterojunction: in this case, a blue-absorbing layer made of α,ω -diphenyl *sexi*-thiophene (P6T) is evaporated on top of the active material as a shield for high energy photons. A thin film (20 nm) of α,ω -bis(biphenyl-4-yl)*ter*-thiophene (BP3T) interposed between P6T and CuPc-C₆₀ avoids the diffusion and possible dissociation of P6T-generated excitons at the interface with the heterojunction.

Besides the possibility of directly selecting organic dyes with suitable absorption spectra, an alternative way to achieve wavelength tunability relies on the exploitation of filter effects possibly occurring in sandwich-like devices. Manifestation of such effects often arises as the consequence of non-uniformities in the spatial distribution of the internal electric field, in the exciton dissociation profile and/or in charge carriers transport.^[112,113] This was shown in a recent paper where variation of the active layer thickness was used to finely tune the spectral responsivity of a P3HT-based photodiode.^[107] Filter effects were exploited to switch from a symbiotic behavior of the photocurrent spectrum, tracking the shape of the absorption spectrum, to an antibatic one, where photocurrent and absorption spectra are almost complementary. Other examples of finely tuned wavelength responsivity in OPD devices based on a similar approach have been reported in the literature.^[114,115] For instance, OPDs with tunable photoresponse based on optical microcavity effects like in a Fabry-Perot resonator have been proposed:^[114] here, a transparent and conductive optical spacer based on molybdenum trioxide (MoO_3) was placed between the active material and the reflective aluminum electrode to simultaneously *i*) address wavelength tunability upon variation of microcavity thickness and *ii*) place the organic D/A heterojunction at the resonant field peak of intensity, thus increasing the responsivity.

4.1.4. Ultraviolet Detectors

UV detectors are usually considered as a niche field, though there is a strong interest both for scientific, commercial, civil and military applications. A few examples are chemical and biological sensing, smoke and fire detection, missile warning, combustion monitoring, ozone sensing, among many others.^[116,117] Si and GaAs technologies saw soon the competitions of more suited materials such as GaN, SiC or diamond^[118–120] which allow to achieve responsivities in the 100–200 mA/W range with a superior UV radiation hardness. Of course the fabrication of detectors with these technologies requires costly processes and therefore organic based UV detectors offer also in this case the opportunity for process simplification and widespread integration of cheap detectors, with anyway a still not fully answered question mark regarding their radiation hardness.

In the literature the most widely adopted structure for organic UV detectors is the vertical one. Most of organic UV detectors are generally matched to the so called UV-A range (310–420 nm),^[116] or near-UV (NUV) range which more or less corresponds. The deep-UV (DUV) range from 350 nm to 190 nm^[117] is much less covered.

For various applications *spectral selectivity* is very important and in particular visible-blind detectors, also referred to as solar-blind devices, have been developed, where the relevant figure of merit is the UV to visible rejection ratio ($R_{\text{UV/Vis}}$). In the NUV range, detectors with a $R_{\text{UV/Vis}}$ of $\sim 10^3$ were demonstrated.^[121–123] This concept is very relevant in the case of DUV, in applications like solar astronomy, inter-satellite communications, missile detection, heat sensing and sterilization monitors.^[124] In organic detectors, selectivity to the DUV radiation has been demonstrated so far only with the adoption of filters placed on top of a semitransparent metallic cathode, where DUV radiation is shined through instead of the ITO anode, since this is not transparent to such high energy photons. Examples are N,N'-diphenyl-N,N'-bis(3-methyl-phenyl)(1,1'-biphenyl)-4,4'-diamine (TPD)^[124] and poly(vinyl alcohol) (PVA) films blended with organic dyes,^[125] where $R_{\text{UV/Vis}} \approx 10^3$ were also obtained.

Concerning the active materials adopted in the UV responsive layer, small molecules are quite common and this usually implies the adoption of vacuum thermal evaporation as the favored deposition method. In the case of donors, large E_G triarylamines derivatives were extensively adopted,^[121,126–128] and among these 4,4',4''-tri-(2-methylphenylphenylamino) triphenylamine (m-MTDATA) is definitely the most common choice. This because m-MTDATA, a well known material in OLEDs applications, combines a relatively high hole mobility of $3 \times 10^{-5} \text{ cm}^2/\text{Vs}$,^[129–131] with a very low Electron Affinity (EA) of 1.9 eV and an Ionization Potential (IP) of 5.1 eV.^[132,133] Other diamine derivatives were adopted, such as a starburst amine,^[134] though yielding a detector not blind to the visible, TPD^[135] and N,N'-bis(naphthalen-1-yl)-N,N'-bis(phenyl)benzidine (NPB).^[123] Overall the variety of donor materials is quite limited, while many more acceptor materials have been tested. 8-hydroxy-quinoline based complexes were tested: co-evaporation of Alq_3 and TPD acting as acceptor and donor respectively is one example.^[135] The device anyway showed a limited responsivity R of $\sim 30 \text{ mA/W}$ at 360 nm (EQE $\sim 10\%$). This is because the IP and EA of Alq_3 , being 5.5 eV and 2.4 eV respectively^[132] are not well matched with TPD levels.^[136] Better performances can be obtained by using tris(8-hydroxyquinoline) gallium (Gaq₃), a complex with energy levels very similar to Alq_3 , but suppressing radiative decay in combination with m-MTDATA.^[132] The m-MTDATA:Gaq₃ blend device showed $R = 338 \text{ mA/W}$ at 365 nm, with an applied bias voltage of 8 V. This level of responsivity is very high and it is associated to an EQE > 100%, indicating a photoconductive behavior.^[81] Both m-MTDATA: Alq_3 and m-MTDATA:Gaq₃ based device are not visible-blind due to a relatively strong absorption in the 400 to 450 nm range. To reduce absorption in the visible, the coordinating metal atom was changed from Ga in favor of various rare earth complexes, and in particular gadolinium, characterized by a blue-shifted absorption.^[128] A 1:1 blend of m-MTDATA and tris-(8-hydroxy-quinoline) gadolinium (Gdq) yielded a detector with a 365 nm

responsivity of 230 mA/W at 7.5 V (EQE \approx 78%), with very suppressed photocurrent above 400 nm. Other successfully adopted acceptors are: bis(2-methyl-8-quinolinato)-4-phenylphenoxy aluminum (BAIq), a common electron transporting layer in OLEDs, characterized by a high electron mobility and a good level matching with m-MTDATA,^[126,136] 1,3,5-tris(N-phenylbenzimidazol-2-yl) benzene (TPBi), a high electron mobility material with a peak absorbance around 315 nm,^[129,130] 1,3,4-oxadiazole-containing oligoaryls, also covalently linked to tryarildiamine compounds,^[121] and 2-(4-tertbutylphenyl)-5-(4-biphenyl)-1,3,4-oxadiazole (PBD).^[123] Wide E_g acceptors, such as 4,7-diphenyl-1,10-phenanthroline-(bathophenanthroline) (Bphen)^[124] or a silane-containing triazine derivative (NSN),^[125] allowed to develop DUV detectors in combination with a proper donor and with the filters mentioned before. In the latter example, solution processing, which finds limited adoption in the case of UV detectors in the literature, was adopted for polymeric donors, such as poly(9,9-dihexylfluorene-2,7-diyl) (PFH) and poly(N-vinylcarbazole) (PVK). These polymers were applied as electron donors and deposited by spin-coating on top of a vacuum deposited NSN acceptor, achieving responsivities comparable to all vacuum-deposited devices (10–100 mA/V in the 250–350 nm range).^[125]

We have collected the performances data related to many organic and hybrid UV detectors in **Table 2**. As it is possible to observe R usually ranges from a few tens of mA/W to several hundreds of mA/W at wavelengths usually located around 350–360 nm with a light intensity which often is \sim 1 mW/cm². For the most responsive devices EQE is usually exceeding 100%, clearly indicating that gain mechanisms typical of photoconductors are active (see Section 2.2.3). Given the photoconducting working principle, concerns may arise regarding the device time response, but unfortunately there is overall very limited data. The fastest devices are characterized by a response time below 400 ns^[121] or even of a few tens of ns,^[127] while usually a milliseconds regime is achieved.

Since many UV applications, in fields such as automotive, aerospace and biology, require stable devices also capable of working in harsh environments,^[116] it is important to discuss whether organic based UV detector can qualify at all for such stringent applications. To date most of the reports do not deal with devices stability, and other reports contain only partial tests up to a maximum 1000 minutes of operation in air under UV light.^[124,126,128] Preliminary data shown in a few reports seem to suggest that organic UV detectors capable of operating for longer time (up to hundreds of hours) should be possible.^[121,134] Further studies under controlled test conditions are therefore needed, though proper encapsulation will definitely be required for harsh environmental conditions.

4.2. Reduction of Dark Currents

Dark currents play a key role in determining the overall performance of a photodetector. More precisely, they should be minimized in order to improve some fundamental aspects like the *power consumption* and the effectiveness of *photocurrent read-out process*, e.g. avoiding saturation of the read-out electronics. Dark currents also affect the efficiency of signal detection by

increasing photogenerated carriers *recombination losses* and by being a major source of *electronic noise*. Indeed, the entity of the electronic noise ultimately sets the sensitivity of a photodetector by determining the minimum detectable amplitude of the impinging optical signal. A commonly adopted figure of merit to quantify the limit of what can be detected due to the presence of noise is the Noise Equivalent Power (NEP), defined as the signal optical power yielding a SNR equal to 1. It can be written as:

$$NEP = \frac{S_{\text{noise}} \cdot \sqrt{\Delta f}}{R} \quad (4)$$

where S_{noise} is the noise spectral density in $A/\sqrt{\text{Hz}}$ and Δf is the BW in Hz. The reciprocal of the NEP is referred to as the *detectivity D* of the device. Besides depending on the signal BW Δf , D also depends on the size of the detector active area (A). Normalization of D with respect to Δf and A is often applied to enable straight comparison of different devices in terms of sensitivity:

$$D^* = \frac{\sqrt{\Delta f \cdot A}}{NEP} \quad (5)$$

D^* is typically referred to as the *specific detectivity* of the detector and it is commonly expressed in Jones, i.e. $\text{cm} \cdot \sqrt{\text{Hz}}$.

Even if many mechanisms can be claimed to be sources of electronic noise inside organic photodetector devices, like Johnson noise, dielectric noise or flicker noise,^[137] the *shot noise* from the dark currents is commonly assumed to be the dominant contribution.^[92] In the frame of this assumption, the expression of D^* becomes:

$$D^* = \frac{R \cdot \sqrt{A}}{\sqrt{2qJ_{\text{dark}}} = \frac{R}{\sqrt{2qJ_{\text{dark}}}} \quad (6)}$$

with J_{dark} the dark current density and $2qJ_{\text{dark}}$ the shot noise power spectral density (S_{noise}).

Although it must be stressed that the topic of electronic noise in organic devices has been scarcely addressed so far and no systematic studies can be found in the literature, noise measurements performed in 2007 by the group of Yang^[91] on PTT:PC₆₁BM BHJ based photodetector indeed revealed a good matching between the device actual noise current and the calculated shot noise contribution, confirming the dark currents as major responsible for the detector noise thus stressing the importance of their reduction.

In order to effectively address dark currents suppression, their ultimate origin has to be identified. Given the relatively large energy bandgap E_g of organic materials, *bulk thermal generation* of carriers can be typically ruled out as a major contribution to the dark currents ($n_i \propto e^{-(E_g/2kT)}$, with n_i the concentration of thermally generated carriers). Thermal generation of carriers at the D/A interface via ground-state charge-transfer interaction can be also typically neglected at least in the case of UV-visible photodetectors, as demonstrated for instance for the case of F8BT-PDI BHJ photodiodes.^[69] On the other side, since photodetector devices are generally operated with an applied bias voltage, charge injection from the metal contacts into the semiconductor can be non-negligible.^[69] Even if an exhaustive model describing the dynamics of charge injection

Table 2. UV photodetectors based on organic semiconductors or hybrid materials.

Method	Active material Device structure ^{a)}	Spectral window	Responsivity @V _{BIAS} (Light source, Intensity)	I _{light} /I _{dark} (V _{BIAS})	t _R ^{b)}	Ref.
Vapor	D2:A2 ^{c,d)} (BHJ)	300–410 nm	220 mA/W @ -8 V (380 nm, 0.072 mW/cm ²)	~10 ² (-2 V)	<400 ns	[121]
	m-MTDATA/Cu(DPEphos) ((Bphen))BF ₄ ^{e,f)} (bilayer)	300–420 nm	62 mA/W @ 0 V (365 nm, 1.7 mW/cm ²)	NA	NA	[204]
	TPD:Alq ₃ (BHJ)	~200–450 nm	30 mA/W @ -15 V (360 nm, 1.4 mW/cm ²)	~10 ⁴ (-15 V)	~1ms	[135]
	m-MTDATA: Gd ₃ (BHJ)	~320–420 nm	338 mA/W @ -8 V (365 nm, 1.2 mW/cm ²)	675 (-8 V)	NA	[132]
	m-MTDATA/TPBi (bilayer)	250–400 nm	75.2 mA/W @ -6.5 V (365 nm, 1.0 mW/cm ²)	3405 (-6.5 V)	NA	[130]
	m-MTDATA/TPBi/Bphen[f] (trilayer)	NA	79.9 mA/W @ 0 V (365 nm, 2.0 mW/cm ²)	NA	NA	[205]
	m-MTDATA/TPBi/Bphen[f] (tandem)	NA	27.3 mA/W @ 0 V (365 nm, 2.0 mW/cm ²)	NA	1.5 ms	[205]
	m-MTDATA/m-MTDATA: Bphen/Bphen/ Cs ₂ CO ₃ :Bphen ^f (with filter)	250–400 nm	309 mA/W @ -8 V (280 nm, 0.428 mW/cm ²)	510 (-8 V)	NA	[124]
	PCATA/Alq ₃ (bilayer)	~300–450 nm	47.1 mA/W @ 0 V (365 nm, 1.02 mW/cm ²)	NA	NA	[134]
	PCATA/TPBi (bilayer)	NA	64.7 mA/W @ 0 V (365 nm, 1.02 mW/cm ²)	NA	NA	[134]
	NPB/PBD (bilayer)	300–420 nm	4.5 A/W @ +3 V (350 nm, 60 μW/cm ²)	~24000 (+3 V)	NA	[123]
	m-MTDATA/TPBi/BCP (trilayer)	300–400 nm	100 mA/W @ 0 V (365 nm, 0.426 mW/cm ²)	NA	NA	[129]
	m-MTDATA: TPBi/BCP (BHJ)	300–400 nm	135 mA/W @ -4 V (365 nm, 0.426 mW/cm ²)	NA	NA	[129]
	m-MTDATA: Gd ₃ (BHJ)	300–400 nm	230 mA/W @ -7.5 V (365 nm, 1.2 mW/cm ²)	260 (-7.5 V)	NA	[128]
	m-MTDATA/NSN (bilayer)	300–410 nm	334 mA/W @ -12 V (365 nm, 1.0 mW/cm ²)	~300 (-12 V)	NA	[125]
	PFP/NSN (bilayer)	300–375 nm	245 mA/W @ -12 V (340 nm, 0.5 mW/cm ²)	10 ²	NA	[125]
	With NUV filter	200–300 nm	19.87 mA/W @ -9 V (270 nm, NA)			
	m-MTDATA/CuPc (bilayer)	300–400 and 550–800 nm	32.1 mA/W @ 0 V (365 nm, 1.7 mW/cm ²)	NA	NA	[206]
	m-MTDATA/(OXDPybm) Gd(DBM) ₃ (bilayer)	300–400 nm	55 mA/W @ 0 V (365 nm, 1.7 mW/cm ²)	NA	NA	[207]
	m-MTDATA/m-MTDATA: BALq/BAlq (BHJ)	300–400 nm	248 mA/W @ -14 V (365 nm, 0.691 mW/cm ²)	NA	NA	
		300–400 nm	514 mA/W @ -7 V (365 nm, 1.2 mW/cm ²)	~10 ³ (-7 V)	NA	
Solution and vacuum	PVK/NSN (bilayer)	300–370 nm	~400 mA/W @ -12 V (340 nm, 0.5 mW/cm ²)	~10	NA	[125]
	With NUV filter	200–300 nm	38.76 mA/W @ -9 V (275 nm, NA)			
	PFH/NSN (bilayer)	300–425 nm	696 mA/W @ -12 V (365 nm, 1.0 mW/cm ²)	498 (-12 V)	NA	[125]

^{a)}In case of bi- or multilayers active materials are separated by a slash, whereas in case of bulk heterojunction active materials are separated by a colon; ^{b)}t_R is the device response time; ^{c)}D2: spirobifluorene-cored triaryldiamine; ^{d)}A2: spirobifluorene-cored oxadiazole-containing hexaaryl; ^{e)}DPEphos: 6,7-dicyanodipyrro[2,2-d:2',3'-f]quinoxaline; ^{f)}Bphen: bathophenanthroline.

at metal/organic interfaces can't be found in the literature, due to presence of secondary effects like energetic disorder, interposition of native oxides or interfacial dipole formation,^[138,139] a strong dependence of the hole (electron) injection rate on the height of the Schottky barrier ϕ_B is expected, where ϕ_B (assuming that the metal Fermi level lies within the semiconductor energy gap) for holes (electrons) is the difference between the metal Fermi level (semiconductor LUMO) and the semiconductor HOMO (metal Fermi level). The lower is ϕ_B , the higher will be the injected dark current (for a more comprehensive description of charge injection phenomena at metal/organic interfaces refer to Ref. [138] and [139]).

In the literature, very low dark currents have been demonstrated for sandwich-like devices with increased inter-electrode spacing, i.e. thickness of the active layer: for instance, dark

currents below 1 nA/cm² have been reported^[61] for photodiodes based on 4 μm thick MEHPPV:PC₆₁BM BHJ. In this specific case, good EQE (~35%) and reasonable photogenerated charge collection efficiency (above 75% at 1 V/μm internal electric field) despite a very large device thickness are enabled by well balanced transport of holes and electrons. Even if careful tuning of the active material thickness might allow in some cases a reasonable compromise between leakage current and EQE to be reached,^[58] suitable engineering of the metal-semiconductor interfaces to suppress charge injection phenomena is generally accounted as a preferable way to address dark currents reduction. More specifically, charge injection phenomena can be significantly suppressed if the Schottky barrier at the metal/semiconductor interface is made high enough. In the case of bulk heterojunction systems, where such energy barriers are

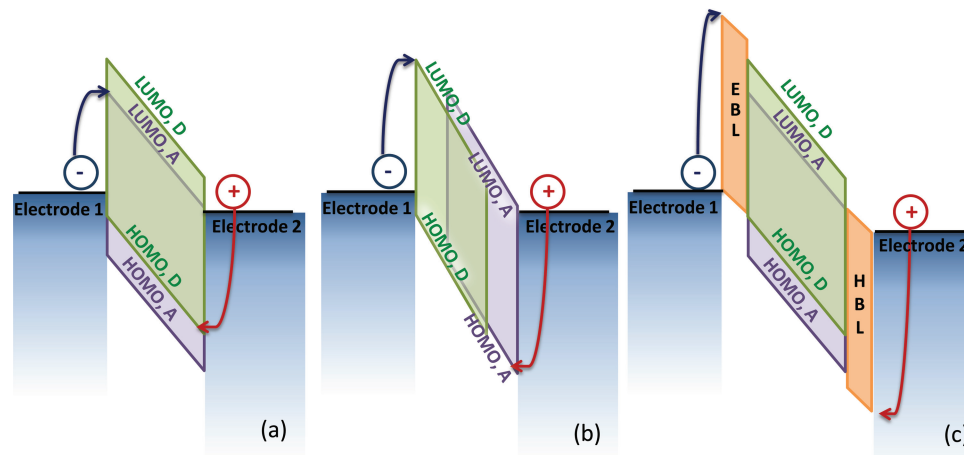


Figure 5. Sketch of charge injection phenomena from the metal contacts into the active material in the case of (a) a generic D/A bulk-heterojunction, (b) a vertically segregated D/A bulk-heterojunction, and (c) a device provided with dedicated injection blocking layers.

typically small and ill-defined due to both the donor and the acceptor species being possibly present at the metal/organic interface (Figure 5a), large improvement can be in principle achieved by controlling donor/acceptor vertical phase segregation (Figure 5b). On this side, it has been shown^[140] that dark current in P3HT:PC₆₁BM photodetectors can be progressively reduced by moving from the as cast bulk heterojunction active material to a double-layer device. As an intermediate step, post deposition treatments like thermal annealing are demonstrated to effectively diminish the leakage likely due to a better contact selectivity induced by changes in the D/A vertical composition profile. However, it must be stressed that direct modification of the active material morphology or composition, while possibly reducing the dark current, can simultaneously affect the responsivity of the device,^[58] thus also limiting the overall benefit in terms of detectivity. Alternatively, extra layers interposed between the metal contact and the active material can be exploited (Figure 5c) to inhibit charge carriers injection. If suitably engineered^[141] so that while charge injection is effectively suppressed, photogenerated carriers collection is not hindered and light is not prevented from reaching the photoactive layer, the blocking layers (BLs) should in principle allow the quantum efficiency of the device to be preserved. Nevertheless, despite being relatively easy to realize in the case of small molecules through thermal evaporation,^[142] multilayered structures are hard to develop by solution processing due to the need of finding orthogonal solvents for successive depositions.^[143] Insolubilization of underlying layers by means of suitable post deposition treatments is often required. One option is to exploit photo-crosslinking of polymers in presence of a suitable photo-crosslinking agent (e.g. bis-fluorinated phenylazide)^[67] in order to develop an all-solution based multilayer device. For the case of an all-solution processed OPD based on P3HT:F8TBT active material, a dark current reduction by two orders of magnitude down to few tens of nA/cm² was demonstrated by introduction of dedicated blocking layers both at the anode side and at the cathode side respectively preventing the injection of electrons (Electron Blocking Layer - EBL) and holes

(Hole Blocking Layer - HBL) into the semiconductor.^[67] Despite the good results achieved in terms of dark current suppression, from the paper clearly emerges the main criticality of multilayer device fabrication by means of film cross-linking: indeed, while the introduction of a cross-linked BL as the first layer of the stack is possible without significant loss in the quantum efficiency thanks to a careful process of material selection and film thickness optimization, on the other hand the deposition of an upper BL on top of the stack, requiring the insolubilization of the underlying photoactive layer, is paid in terms of device EQE. However, despite these technological issues requiring careful optimization, the BL-based dark current suppression technique is proved to be a promising way to increase the detectivity of organic photodetectors. Indeed, it plays even a more strategic role when it comes to bulk-heterojunction systems embedding low bandgap compounds, the Schottky barriers becoming correspondingly smaller. As far as small bandgap materials, even through direct thermal generation of carriers and cross-generation (through ground-state charge-transfer reactions) at the D/A interface can arise as concurrent non-negligible contributions to the dark current, charge injection phenomena still have a major part. Successful reduction of dark current by introduction of spin-coated polystyrene-N,N-diphenyl-N,N-bis(4-n-butylphenyl)-(1,10-biphenyl)-4,4-diamine-perfluorocyclobutane (PS-TPD-PFCB) EBL and thermally evaporated C₆₀ HBL was demonstrated^[92] for photodetectors based on the low bandgap polymer PDDTT in bulk-heterojunction with PC₆₁BM. Specific detectivity D^* higher than 10^{12} cmHz^{1/2}/W at 800 nm, comparable to that of standard Si- and InGaAs-based detectors, was achieved. More recently, a solution processed squaraine:PC₆₁BM bulk-heterojunction photodetector was demonstrated^[82] where dark currents are reduced by a factor of 30 thanks to the introduction of a UV-light crosslinked MEHPPV layer acting as the EBL. As a result, specific detectivity of $3.4 \cdot 10^{12}$ cmHz^{1/2}/W at 700 nm was reached. Notably enough, being of general validity at least in the case of injection dominated dark current, the BL-based approach has been applied with good success also in devices made of inorganic nanostructured active materials: as

an example, an increase of D^* by one order of magnitude (up to $10^{12} \text{ cmHz}^{1/2}/\text{W}$ at 600 nm) was demonstrated by introduction of poly[(9,9'-dioctylfluorenyl-2,7-diyl)-co-(4,4'-(N-(4-sec-butyl)diphenylamine)] EBL and zinc oxide nanocrystals HBL in photodetectors based on solution processed PdSe quantum dots acting as the photoactive medium.^[144]

5. Phototransistors

5.1. Small Molecular Phototransistors

5.1.1. Vacuum Deposited Small Molecules

The first few reports which introduced OPTs with conjugated small molecules or polymers^[145–148] did not attract much attention because performances of those OPTs, such as R , the ratio of photocurrent to dark current (I_{ph}/I_{dark}), and the charge carrier mobility, were relatively lower than those for inorganic phototransistors.^[145–148] Meanwhile, Noh et al. developed a significantly improved OPT based on 2,5-bis-biphenyl-4-yl-thieno[3,2-b] thiophene (BPTT) (see chemical structure in Figure 6). As shown in Figure 7, the BPTT OFETs showed a μ_{FET} of $0.082 \text{ cm}^2/\text{Vs}$, and the measured maximum R and the I_{ph}/I_{dark} were 82 A/W and 2.0×10^5 , respectively.^[149] Under UV light illumination, the channel current was increased to $20 \mu\text{A}$ at $V_g = -20 \text{ V}$ by photovoltaic effect. The increase in photo-current in BPTT OPTs over the dark current is about 100 times higher than those of previously reported OPTs and even higher than what reported for amorphous silicon based phototransistors.^[149] Moreover, it was reported that the operating mechanism of OPT is similar to that of inorganic phototransistors.

Later, the same group reported high performance OPTs with well-known small molecular organic semiconductors, such as pentacene or CuPc. The pentacene and CuPc OPT exhibited photosensitivity of $10\text{--}50 \text{ A/W}$ and $1.5\text{--}2.4 \text{ A/W}$, respectively. The most interesting result by Noh et al. is that the relationship between photocurrent and absorption spectra showed antibatic behavior, with the maximum of the photocurrent obtained at the minimum of the absorbance, owing to an internal filtering effect.^[150] This is due to the fact that in the chosen device architecture the nanometer thin accumulated channel, which develops at the semiconductor-dielectric interface, is buried underneath the rest of the semiconductor layer. The light impinging on the device has first to pass through the non-accumulated bulk semiconductor, which acts only as an optical filter, before reaching

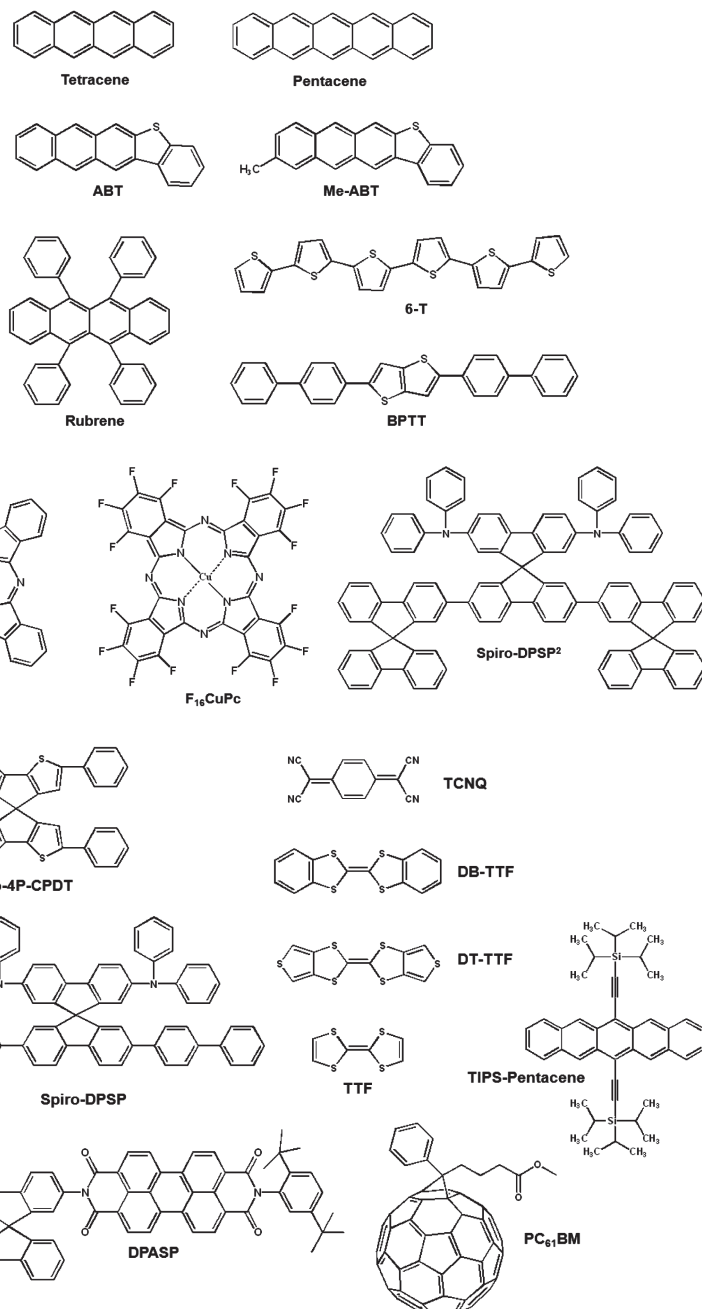


Figure 6. The small molecular semiconductors commonly used in OPTs. Reproduced with permission from Ref. [199]. Copyright 2010, Wiley-Interscience.

the channel. Therefore, the shape of the incident photon conversion efficiency (IPCE) spectrum is strongly affected by the absorption spectrum (Figure 8).^[150]

In a comparative study of the photo-response between tetracene- and pentacene-based OFETs, the tetracene FETs showed superior potential as a OPT in the visible and UV light range, although it exhibited two orders of magnitude lower field-effect mobility ($0.003 \text{ cm}^2/\text{Vs}$) than that of pentacene FETs ($\sim 0.3 \text{ cm}^2/\text{Vs}$).^[151] The tetracene devices showed higher photocurrent ($\sim 30 \text{ nA}$) than the pentacene devices ($\sim 1 \text{ nA}$) in the depletion

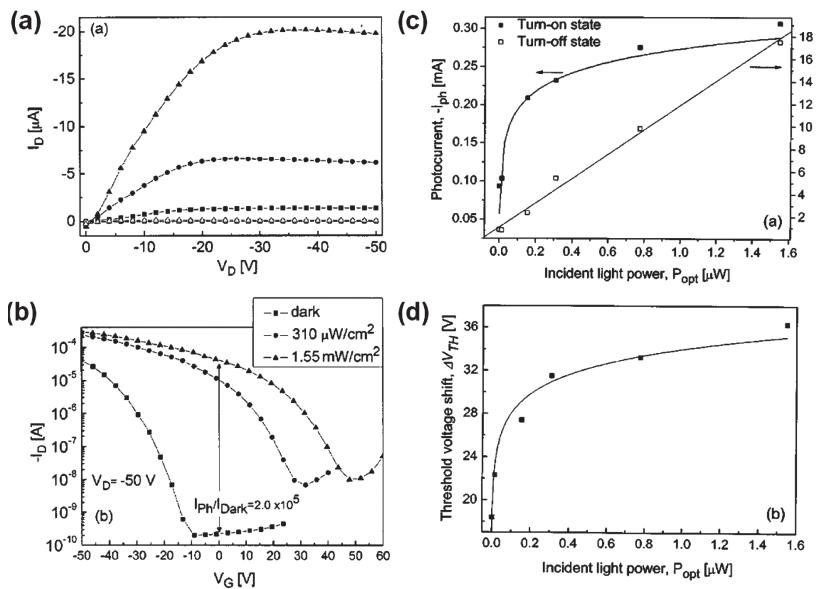


Figure 7. (a) Output characteristic of OPTs measured in the dark (open symbols) or under UV irradiation (closed symbols) with 1.55 mW/cm^2 at different V_g . (b) Transfer characteristics of the BPTT OPTs measured in the dark (closed squares) or under UV with $310 \mu\text{W}/\text{cm}^2$ (closed circles) and $1.55 \text{ mW}/\text{cm}^2$ (closed triangles) at $V_d = -50 \text{ V}$. (c) Photocurrent as a function of incident light power under turn-on ($V_g = -50 \text{ V}$, closed squares) and turn-off (minimum I_d , open squares) states at $V_d = -50 \text{ V}$. (d) The threshold voltage shift as a function of incident light power of the BPTT OPTs. Symbols denote measured data points and the solid lines indicate fitted results using Eqs. (1) and (2). Reproduced with permission from Ref. [149]. Copyright 2005, American Institute of Physics.

region, thus displaying a much higher I_{ph}/I_{dark} ratio (3×10^3) than pentacene device (~10). This different photo-response behavior can be attributed to the fact that photo-absorption (or photo-generated exciton density) of the tetracene film was much higher than that of the pentacene film with identical thickness, and more importantly, the exciton life time in solid tetracene is much longer (~200 ps) than in solid pentacene film (~1 ps).^[151]

Typical organic materials, such as pentacene and tetracene, are indeed not suitable for OPTs, because the former has high mobility and relatively low light-sensitivity, while the latter

exhibited a low mobility and a high sensitivity. Since organic semiconductors play a key role to determine the performance of OPTs, it is important to develop organic semiconductors both with high mobility and excellent light sensitivity. To this extent, Liu et al. reported high efficiency OPT devices using an asymmetric organic semiconductor, anthra[2,3-b]benzo[d]thiophene (ABT), in which the ABT molecules are packed similarly to pentacene, producing an efficient charge transport and simultaneously exhibit a similar absorbance to that of tetracene, resulting in high photo-sensitivity.^[152] The ABT-based OPTs showed a high mobility of $0.4 \text{ cm}^2/\text{Vs}$, good photo-responsivity of ca. 10^3 A/W , large I_{ph}/I_{dark} of ca. 800, and excellent air-stability over a few hundred of days timescale. It was noted that the mobility is not changed under light irradiation, but the maximum values of R and I_{ph}/I_{dark} of the OPTs increased with increasing the gate voltage V_g . This can be explained as an effect of the vertical electric field on the exciton separation efficiency.^[152]

Most of OPT devices reported so far have been based on inorganic gate dielectrics, typically SiO_2 . Cost-effective polymeric gate dielectrics can be considered as better candidates to demonstrate commercially appealing

organic optoelectronic devices and circuits. Poly(4-phenoxyethyl styrene) (P4PMS) and cross-linked poly(4-vinyl phenol) (CL-PVP) were utilized by Pyo et al. to fabricate n-type F_{16}CuPc -based OPT devices.^[153,154] It was noted that the rigid, planar molecular structure of a molecule such as F_{16}CuPc , typically results in large internal conversion quantum yields and high photocurrent densities owing to the more effective absorption of incident light compared to molecules with three-dimensional complex structures.^[153] The F_{16}CuPc OPT device showed a photo-responsivity of 1.5 mA/W with a short rising time of

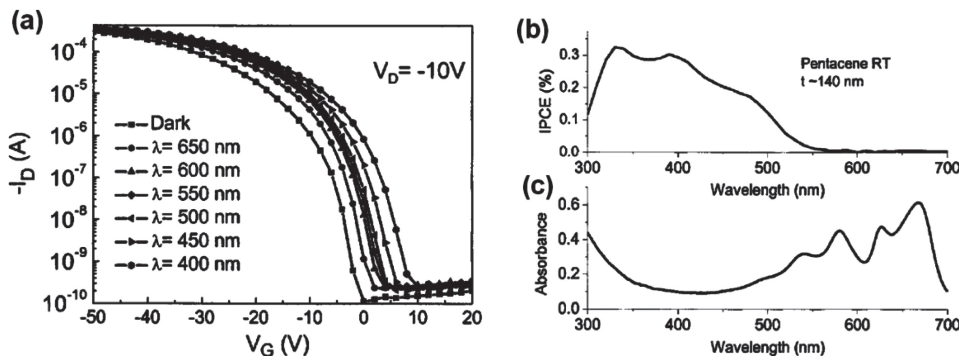


Figure 8. (a) Transfer characteristics of the pentacene OPTs measured in the dark (closed squares) or under a xenon lamp at an intensity of $5 \text{ mW}/\text{cm}^2$ with color filters of 650, 600, 550, 500, 450 and 400 nm to obtain monochromatic light at $V_d = -10 \text{ V}$. (b) IPCE (%) for ITO/pentacene(140 nm)/Al device and (c) the UV-Vis absorption spectrum of a pentacene film (140 nm). Reproduced with permission from Ref. [150]. Copyright 2005, American Institute of Physics.

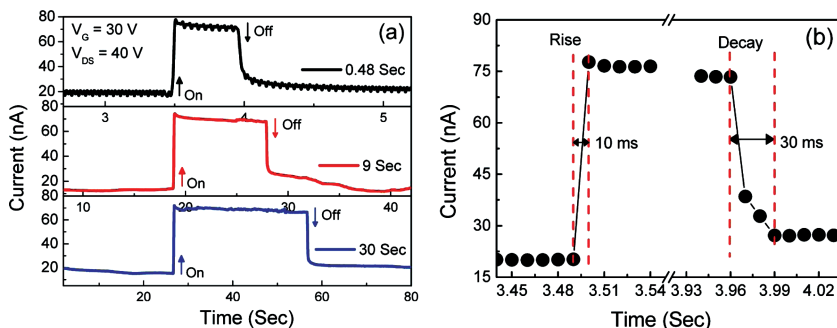


Figure 9. (a) Transient behavior of I_d response to different illumination times. Optical pulse (5.66 mW/cm^2) was turned on for 0.48, 9, and 30 s with fixed $V_g = 30 \text{ V}$ and $V_d = 40 \text{ V}$. Turning on/off the light is indicated by arrows. (b) Enlarged view of rise and decay of photocurrent. The data were obtained from panel a for 0.48 s pulse duration. Reproduced with permission from Ref. [153]. Copyright 2010, American Chemical Society.

much less than 10 ms (Figure 9). This rising time, which can be strongly improved, is sufficiently short for opto-electronic applications such as UV and visible light detectors. However, it is interesting to note that the decay time is even longer (measured decay time was ca. 30 ms); this can be ascribed to the slow nature of the recombination of generated charge carriers because of the poor recombination cross section of the trapped holes within the intrinsic region in the presence of an electric field.^[153] The photo-responsivity and photo-switching speed of the OPT were similar with two dielectric materials, CL-PVP and P4PMS, but the mobility and stability of the OPT were found to be the better for P4PMS than CL-PVP,^[154] presumably due to interfacial electron traps in CL-PVP. In addition, by suitably combining optical and electrical pulses, various opto-electronic functions were demonstrated, such as photo-detection, photo-switching, multi-level data recording, and signal amplification.^[154]

Spiro-conjugated organic molecules have been extensively studied in various organic optoelectronic devices, such as OLEDs, OPVs, OFETs, and OPTs.^[155–157] Saragi et al. first demonstrated an intramolecular charge transfer in spiro-type molecules, 2,7-bis-(N,N'-diphenylamino)-2',7'-bis(biphenyl-4-yl)-9,9'-spirobifluorene (Spiro-DPSP), which led to a photoconductive effect.^[156] It is noted that a charge transfer between the molecular halves, which leaves a positive charge in the amine moiety and a negative charge in the sexiphenyl chromophore in Spiro-DPSP, is more favorable in more polar environments. Since hole transport via hopping between the bis(diphenylamino)biphenyl sites is faster than electron transport, the Spiro-DPSP can be regarded as an ideal photoconductor in which every excitation center of the one-component system carries its own electron trap. Therefore, this system can be considered to fulfill the prerequisite for applications, such as photo-refractive systems or phototransistors, without the need of a heterojunction for efficient charge separation in OPTs. By comparison to symmetrically

substituted parent compounds, such as 2,2',7,7'-tetrakis(diphenylamino)-9,9'-spirobifluorene (Spiro-TAD) which showed no photocurrent, it was possible to show that the bipolar character of Spiro-DPSP, the intramolecular charge transfer and the consequent high yield for exciton dissociation are strictly related.^[156] The Spiro-DPSP OPT devices exhibited a R value of $\sim 1 \text{ A/W}$ under illumination of 370 nm wavelength UV light, and $I_{ph}/I_{dark} \approx 5 \times 10^2$. By using larger spiro-compound, 2,7-bis-(N,N'-diphenylamino)-2',7'-bis(spirobifluorene-2-yl)-9,9'-spirobifluorene (Spiro-DPSP²), OPTs showed higher I_{ph}/I_{dark} (ca. 2.1×10^3).^[157] Moreover, a thiophene unit was introduced into the spiro-structure in order to improve R . The 2,2',6,6'-tetraphenyl-4,4'-spirobi[cyclopenta[2,1-b;3,4-b']dithiophene (Spiro-4P-CPDT)-based OPTs exhibited a higher hole mobility ($1 \sim 2 \times 10^{-4} \text{ cm}^2/\text{Vs}$) and higher R (25 A/W) than those of previously reported spiro-compounds. The responsivity of 25 A/W is the highest value obtained in the case of amorphous organic semiconductors.^[155]

For the adoption of OPTs in low-cost and large area optoelectronic devices, photo-sensitive organic molecules have to be soluble in common organic solvents. In contrast to the vapor-deposited small molecular semiconductors, Joo et al. demonstrated highly photo-responsive OPT devices using soluble star-shaped oligothiophenes with four-armed π -conjugation paths: 1,2,4,5-tetra(50-hexyl-[2,20]-bithiophenyl-5-vinyl)-benzene (4(HPBT)-benzene), and 1,2,4,5-tetra(50-hexyl-[2,20]-terthiophenyl-5-vinyl)-benzene (4(HP3T)-benzene) (see chemical structure in Figure 10).^[158] The measured maximum R was up to 4300 A/W (at $V_g = 0 \text{ V}$) and typically showed more than 2500 A/W even with low incident light power ($<30 \mu\text{W/cm}^2$), as well as a relatively high I_{ph}/I_{dark} of $\sim 4 \times 10^4$ and a relatively short response time (<1 s). These high OPT

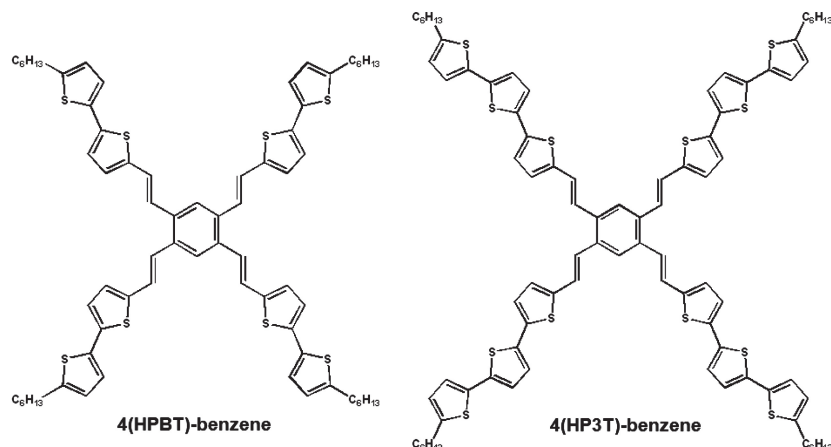


Figure 10. The star-shaped oligothiophenes commonly used in OPTs. Reproduced with permission from Ref. [199]. Copyright 2010, Wiley-Interscience.

performances, which are even higher than those of amorphous Si-based phototransistors ($R \approx 300$ A/W, $I_{on}/I_{off} = 10^3$), are attributed to their unique star-shaped molecular structure. It is noted that the planar core parts with four-armed π -conjugation in these molecules lead to effective absorption of incident light and efficient photo-generation.^[158] Moreover the slow relaxation of the photo-induced charges could lead to reproducible and photo-switched OFET-based memory applications.

Saragi et al. applied D/A assembled molecular system to fabricate solution-processed (SwaOTAD-C₆₀)^[159] or vacuum deposited (DPASP) OPT devices.^[160] D/A dyads as active thin film layers in OPTs showed relatively low electron and hole mobilities of 10^{-6} – 10^{-7} cm²/Vs due to the amorphous thin film morphology. Meanwhile, the SwaOTAD-C₆₀ and DPASP OPTs exhibited the maximum R and I_{ph}/I_{dark} of 0.3 A/W, 0.2 A/W, 115, and 100, respectively. These values are comparable to those of spiro-compounds and CuPc, but lower than those of pentacene and oligothiophene derivatives.^[159] Inkjet-printed OPT devices based on 6,13-bis(triisopropylsilylithynyl) (TIPS) pentacene thin films were investigated by Park et al.^[161] The TIPS-pentacene OPTs showed very high photocurrent modulation (I_{ph}/I_{dark}) of 10^6 – 10^7 due to low off current (10^{-13} A) and sharp subthreshold slope by employing suspended-top-contact structure. Upon illumination the I_d increased up to 10^{-8} A in the off state showing high I_{ph}/I_{dark} , while in the strong accumulation region the current modulation was nearly unity since the number of photo-generated charge carriers was comparable to that accumulated by field-effect.^[161]

The majority of devices demonstrated to date operate at high voltages, typically exceeding 20 V, whereas most targeted applications of OPTs, such as portable and battery-powered optical sensors, ideally require low-voltage sensors.^[162] To this end, Anthopoulos et al. demonstrated the first low-voltage operated and low-power ambipolar OPTs based on pentacene/[6,6]-phenyl-C₆₁-butyric acid methyl ester (PC₆₁BM) heterostructure as the semiconducting layer and a self-assembled monolayer (octadecylphosphonic acid) as the gate dielectric (Figure 11). These transistors were shown to operate below |3| V with electron and hole mobilities on the order of 0.1 and 10^{-3} cm²/Vs, respectively. It was noted that the I_d is dependent not only on the biasing conditions but also on the intensity of incident light, allowing the devices to be used as phototransistors, whose EQE and response time were obtained to be ~0.8% and 210–225 ms, respectively. More interestingly, through the combination of two of such ambipolar OPT devices, low-voltage, light-sensitive complementary-like integrated circuits such as voltage inverters were demonstrated.^[162]

5.1.3. Single Crystal OPTs

Organic single crystal transistors are typically used for investigating intrinsic optoelectronic properties of the semiconducting molecules and for fabricating high performance devices and integrated circuits.^[163] In a few cases organic single crystals were applied for development of high quality OPT devices, in which the nano-/micro-sized organic crystals are synthesized by physical vapor transport (PVT) or solution

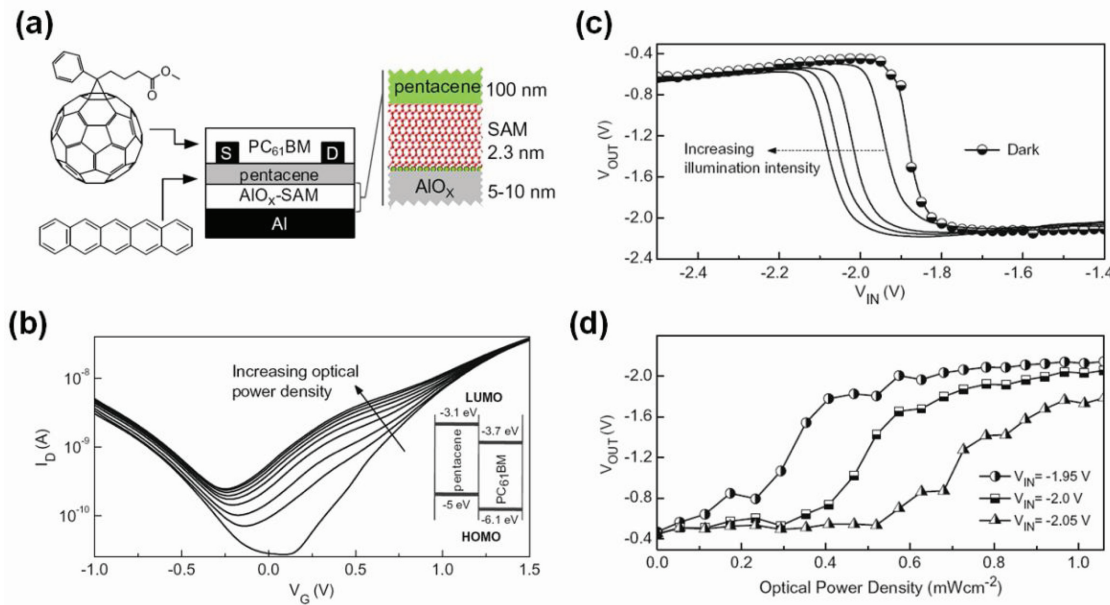


Figure 11. (a) Molecular structures of PC₆₁BM and pentacene and a schematic representation of the bottom-gate, p–n heterostructure transistor. (b) Transfer characteristics of heterostructure ambipolar OFET ($L = 50$ μ m, $W = 1$ mm) measured at $V_d = -1$ V, under blue light illumination (using a $\lambda_{peak} = 469$ nm LED) with incident optical power densities between 0 and 3.2 mW/cm². Inset: simplified energy diagram of the pentacene/PC₆₁BM interface. (c) Transfer characteristics of a low-voltage inverter measured in the dark and under blue light ($\lambda_{peak} = 469$ nm) illumination with incident optical power densities between 0 ~ 1.2 mW/cm². (d) Effect of incident optical power density on V_{out} measured at a fixed V_{DD} (-2.5 V) and different V_{in} biases. Reproduced with permission from Ref. [162]. Copyright 2010, Elsevier B.V.

growth methods. Typically air-stable, n-type semiconductor, copper hexadecafluorophthalocyanine ($F_{16}CuPc$) sub-micro/nanometer ribbons were grown with PVT technique and exhibited high quality OPT characteristics.^[164] With no gate bias applied, the $F_{16}CuPc$ single crystal devices performed as photo-switches having reversible and fast switching speed of 10–20 ms. It was noted that those devices worked as OPTs with a gate connection. The maximum I_{ph}/I_{dark} of the OPTs was 4.5×10^4 , nearly two-three orders of magnitude higher than photoswitches due to efficient separation of the photo-generated excitons into electrons and holes under the gate electric field. A variety of potential applications, such as opto-isolators, highly sensitive optical switches and integrated circuits, were demonstrated using single crystalline based $F_{16}CuPc$ OPTs.

Solution-phase self-assembly processed nano-/micrometer ribbons of a novel linear asymmetric oligoarene, 6-methyl-anthra[2,3-b]benzo[d]thiophene (Me-ABT), were reported by Liu et al.^[165] The individual Me-ABT single crystal-based OPT device exhibited a very high phototransistor performance, such as a high field-effect mobility of $1.66 \text{ cm}^2/\text{Vs}$, a large photo-responsivity of $1.2 \times 10^4 \text{ A/W}$ and I_{ph}/I_{dark} of 6×10^3 even under conditions of low light power ($30 \mu\text{W}/\text{cm}^2$). The record photosensitivity of the OPT device can be attributed to the intrinsic optoelectronic properties of Me-ABT single crystal, in particular the lifetime of excitons, in the range of 0.7–5 ns, which is higher than in pentacene (~1 ps) and in tetracene (~0.2 ns) and it is enough to allow an efficient separation into free charges before decaying by application of V_g and V_d .^[166] It is noted that the high degree of order within the crystals and the absence of grain boundaries are important factors in improving charge carriers mobility and light sensitivity with respect to thin films. The Me-ABT OPTs with the higher ordered structures also showed a higher photocurrent with similar dark current, concomitantly with efficient exciton dissociation and fast travelling of free charges, thus giving rise to higher R .^[165]

A variety of tetraphiafulvalene (TTF) derivatives, such as dithiophene-TTF (DT-TTF) and dibenzo-TTF (DB-TTF), are also well-known materials for easily growing single crystals from solution and have been demonstrated to show relatively high field-effect mobilities. DT-TTF-based OPTs with a field-effect mobility of $0.4 \text{ cm}^2/\text{Vs}$ were fabricated and showed very high I_{ph}/I_{dark} ratio of 10^4 in the transistor off state, in which the photo-induced charge carrier density is $\sim 2.3 \times 10^{16} \text{ cm}^{-3}$.^[167] Meanwhile, the OFET devices based on a DB-TTF single crystal exhibited similar behavior under light illumination, but had much lower I_{ph}/I_{dark} ratio of ~3 because the DB-TTF devices were not completely depleted even when applying a high positive gate bias. In addition, these DT-TTF and DB-TTF OPTs could also be interesting as organic opto/electronic memory elements. The devices showed some persistent (hours time-scale) photocurrent upon illumination (write) even after turning off the light, but this remnant photocurrent can be effectively removed by the application of a high reverse gate voltage (erase).^[167] The photo-controlled memory property can also be applied to multi-state optoelectronic transistor memory devices. Single crystal compounds, which consist of anthracene core and contain two 2-ethynyl-5-hexylidithieno[3,2- b:2',3'-d]

thiophene (DTT) (A-EHDTT) groups in the 9,10-positions of the anthracene core, formed unambiguous J-aggregates and showed high photoresponsivity, exceeding $1 \times 10^4 \text{ A/W}$ under very low light intensity ($1.4 \mu\text{W}/\text{cm}^2$).^[168] OPTs based on crystalline microplates of A-EHDTT showed reproducible multi-stage memory operation characteristics, mainly due to the slow relaxation and trapping of the photo-induced charges. Figures of merits of most relevant small molecule based OPTs are reported in Table 3.

5.2. Polymer Phototransistors

Polymeric optoelectronic devices can be fabricated by cost-effective printing processes, and have excellent compatibility with plastic substrates. These promising features can lead to low-cost and large-area optoelectronic integrated circuits using the various polymer semiconductors (Figure 12). The first OPT device based on a polymer semiconductor was introduced by Narayan et al., where poly(3-octylthiophene-2,5-diyl) (P3OT) and PVA were used as the active channel and gate dielectric layer, respectively.^[169] These devices exhibited a larger $I_{d,ph}/I_{d, dark}$ of ~100 under light illumination (photon flux rate $\sim 1 \mu\text{W}$) than that of organic planar two-terminal photo-detectors (~1.4) due to an additional contribution of the gate electric field. It was also expected that R at low-light levels in the transistor devices can easily be increased to 100 A/W by optimizing the transistor geometry parameters and improving the purity of the active medium.^[169]

Following on this pioneering result, they revealed build up and decay mechanisms of the photo-induced charge carriers (PCCs) in OPTs based on poly(3-hexylthiophene) (P3HT) as the active layer.^[170] The electric field distribution in the device promotes the separation of the PCC. In a p-channel device, the more mobile positive charges drift towards the channel whereas the negative charges find their minimum potential in the bulk and get localized in the trap sites.^[170] The build-up of photo-induced current $I_{on}(t)$ exhibited a logarithmic dependence on time, which implies a spatial separation of PCCs at the interface between p-channel and the bulk according to the model given by Queisser et al.^[171] The photocurrent rise time is faster for more negative V_g (in p-type OPTs), which is primarily attributed to the higher drift/diffusion rates of the photo-generated holes from the bulk to the channel region, and of photogenerated electrons towards the bulk.^[170] Meanwhile, the current decay $I_{off}(t)$ can be fitted forcefully to stretched exponential behavior (Kohlrausch's law)^[170]; the conductivity is given by Equation (7).

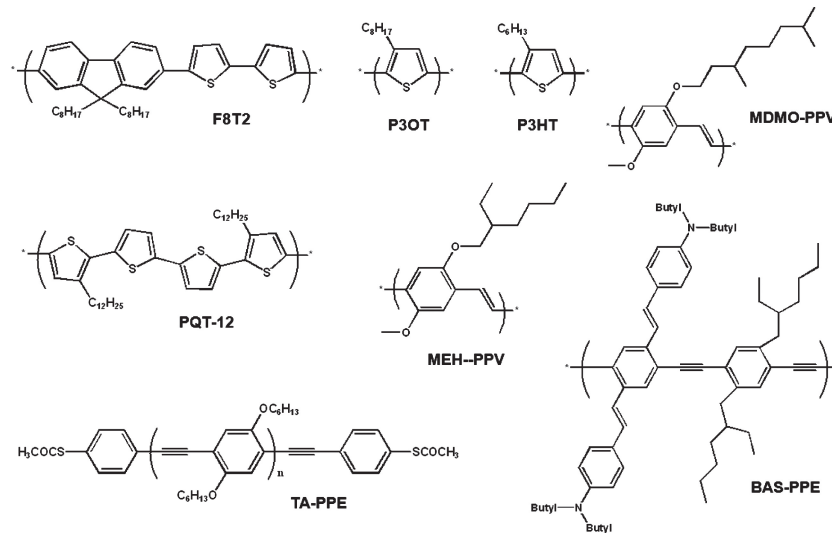
$$\sigma(t) = \sigma_0 \exp \left[- \left(\frac{t}{\tau} \right)^\gamma \right] \quad (7)$$

where, τ is the relaxation lifetime and the exponent γ is indicative of the degree of disorder and is associated with a distribution of activation energies. A modified mechanism was proposed based on serial relaxation dynamics, which involves a hierarchy of systems with increasing spatial separation of the photo-generated negative and positive charges.^[170]

Hamilton et al. have studied OPTs based on [poly(9,9-diocetylfluorene-co-bithiophene)] (F8T2) under steady-state white

Table 3. OPTs based on small molecular semiconductors.

Method	Semiconductor	Structure (Dielectric)	Mobility [cm ² /Vs]	Responsivity (Light source, Intensity)	$I_{d,ph}/I_{d,dark}$	t_R^a	Ref.
Vapor	BPTT	BG/TC (SiO ₂)	0.082	82 A/W (380 nm, 1.55 mW/cm ²)	2×10^5	NA	[149]
	CuPc	BG/TC (SiO ₂)	0.02	0.5–2 A/W (365 nm, 1.55 mW/cm ²)	3×10^3	NA	[150]
	$F_{16}CuPc$	BG/TC (P4PMS)	5.3×10^{-4}	1.5 mA/W (White light, 5.66 mW/cm ²)	22	10 ms	[153]
		TG/BC (CL-PVP)	1.05×10^{-4}	1.4 mA/W (White light, 5.98 mW/cm ²)	79	10 ms	[154]
	Pentacene	TG/BC (CL-PVP)	4.6×10^{-4}	2.15 mA/W (White light, 5.66 mW/cm ²)	300	0.1 s	[208]
		BG/TC (SiO ₂)	0.49	10–50 A/W (365 nm, 1.55 mW/cm ²)	1.3×10^5	NA	[150]
	6T	BG/TC (PMMA)	0.01	0.015 A/W (365 nm, 7 mW/cm ²)	2×10^4	0.1 s	[209]
		BG/TC (SiO ₂)	0.09	1.5–2.4 A/W (365 nm, 1.55 mW/cm ²)	1.3×10^3	NA	[210]
	Tetracene	BG/TC (SiO ₂)	0.003	NA (364 nm, 0.64 mW/cm ²)	3×10^3	NA	[151]
	ABT	BG/TC (SiO ₂ , OTS)	0.4	1000 A/W (White light, 30 μ W/cm ²)	800	NA	[152]
Single Crystal	DPASP	BG/BC (SiO ₂ , HMDS)	$0.67 \sim 6.8 \times 10^{-7}$	0.1 A/W (White light, 0.96 mW/cm ²)	100	NA	[160]
	Spiro-DPSP	BG/BC (SiO ₂ , HMDS)	1.3×10^{-6}	1 A/W (370 nm, 191 μ W/cm ²)	5×10^2	1.5 s	[156]
	Spiro-DPSP ²	BG/BC (SiO ₂ , HMDS)	2.7×10^{-7}	0.44 A/W (370 nm, 64 μ W/cm ²)	2.1×10^3	NA	[157]
	Spiro-4P-CPDT	BG/BC (SiO ₂ , HMDS)	$1 \sim 2 \times 10^{-4}$	25 A/W (370 nm, 2.4 μ W/cm ²)	290	NA	[155]
	Me-ABT	BG/TC (SiO ₂ , OTS)	1.66	12000 A/W (White light, 30 μ W/cm ²)	6000	NA	[165]
	$F_{16}CuPc$	BG/TC (SiO ₂)	0.1	NA (White light, 1.12 mW/cm ²)	4.5×10^4	10 ms	[164]
	DT-TTF	BG/BC (SiO ₂)	0.4	NA (White light, 2.5 W/cm ²)	$\sim 10^4$	NA	[167]
Solution	DB-TTF	BG/BC (SiO ₂)	0.1	NA (White light, 2.5 W/cm ²)	~ 3	NA	[167]
	A-EHDTT	BG/TC (SiO ₂ , OTS)	$1.2 \sim 1.6$	$> 1.4 \times 10^4$ A/W (400nm, 1.4 μ W/cm ²)	1.4×10^5	~ 15 s	[168]
	PY-4(THB)	BG/TC (SiO ₂ , OTS)	0.7	~ 2000 A/W (400nm, 5.6 μ W/cm ²)	1.2×10^6	NA	[211]
	4(HPBT)-benzene	BG/BC (SiO ₂)	0.0013	2500 ~ 4300 A/W (436 nm, 6.8 ~ 30 μ W/cm ²)	4×10^4	< 1 s	[158]
Vapor/ Solution	4(HP3T)-benzene	BG/BC (SiO ₂)	NA	~ 390 A/W (436 nm, ~ 6.8 μ W/cm ²)	NA	NA	[158]
	Swa-OTAD-C ₆₀	BG/BC (SiO ₂ , HMDS)	1.8×10^{-6}	0.3 A/W (370 nm, 1.4 μ W/cm ²)	115	NA	[159]
	Tips-Pentacene	BG/S-TC (cPVP)	0.02	NA (9 ~ 13 mW/cm ²)	$10^6 \sim 10^7$	NA	[161]
Vapor/ Solution	Pentacene/PC ₆₀ BM	BG/BC (ODPA)	$0.1 \sim 10^{-3}$	NA (469 nm, 3.2 mW/cm ²)	$\sim 10^2$	210 ms	[162]

^a t_R is the device response time.

Figure 12. The polymer semiconductors commonly used in OPTs. Reproduced with permission from Ref. [199]. Copyright 2010, Wiley-Interscience.

light irradiation.^[172,173] The off-state I_d of the OPTs is significantly increased due to the illumination, while a relatively smaller effect is observed on the I_d in the strong accumulation regime. The devices showed $R = 0.7$ mA/W (in the strong accumulation regime),^[172] and V_g -independent $I_{d,ph}/I_{d,dark}$ of 10^3 in the off state. As the illumination irradiation increased from 0 to 2.9 mW/cm², the V_{Th} was changed by ~ 10 V, without affecting the value of field-effect mobility and subthreshold swing. Moreover, full recovery of the device to the initial transfer curves was observed after removal of illumination. Recently, the F8T2-based OPT devices were demonstrated to reach very high light sensitivity, in which the maximum R value was as high as 18.5 A/W at 5 μ W/cm² light intensity.^[174] In these devices, the transistor off-current was increased (PCC density changed from 5×10^{11} to 1×10^{13} cm⁻²) with light

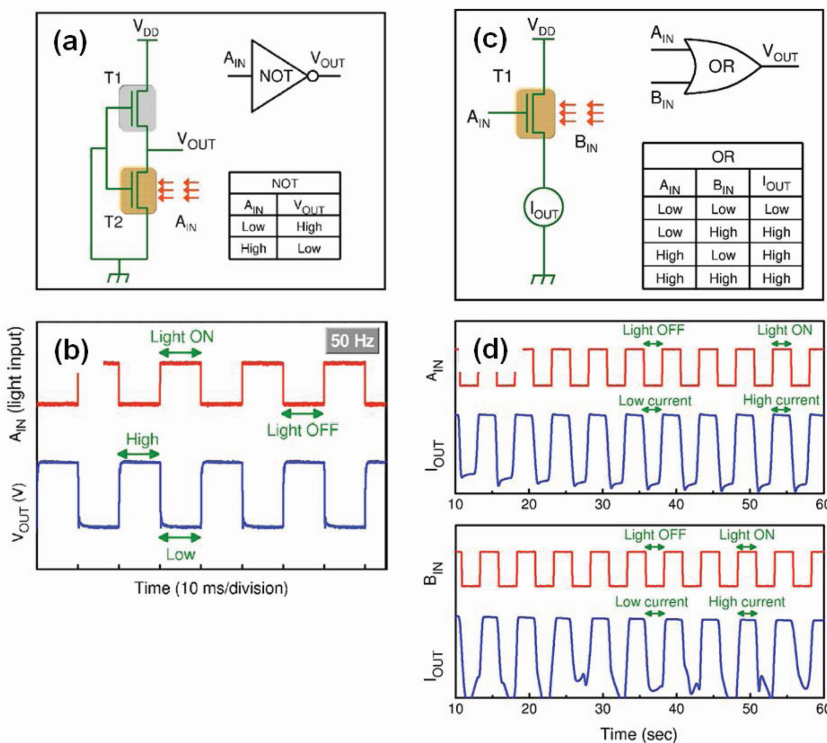


Figure 13. (a) Circuitry of the electro-optical NOT gate together with its symbolic representation and the truth table. (b) Optical input A_{IN} pulsed at 50 Hz (red trace) and the evolution of the output voltage V_{OUT} (blue trace) in time. (c) Circuitry of the electro-optical OR gate together with its symbolic representation and the truth table. The circuit combines two inputs, one electrical (A_{IN}) and one optical (B_{IN}). (d) I_{OUT} , A_{IN} , and B_{IN} versus time. Reproduced with permission from Ref. [178]. Copyright 2007, American Institute of Physics.

intensity (photoconductive effect), meanwhile the on-current increased due to shift in the V_{Th} (photovoltaic effect). Interestingly the initial large contact resistance of the F8T2 OFET device under dark condition rapidly decreased with increasing light intensity.

Rigid-rod conjugated polymers have also been used as an active component in OPTs. Berger et al. reported the OPT devices based on 5-bis(dibutylaminostyryl)-1,4-phenylene-b-alkyne-b-1,4-bis(2-ethylhexyl)benzene terpolymer (BAS-PPE). BAS-PPE is a photoluminescent conducting polymer with a band gap of 2.25 eV, thus ideal for visible light absorption and emission.^[175] R and I_{ph}/I_{dark} ratio values of the BAS-PPE OPTs were reported to be ~ 5 mW/A and 6×10^3 at an incident light intensity of $4 \mu\text{W}/\text{cm}^2$. Hu et al. reported an OPT with a rigid-rod conjugated polymer, a derivative of poly(*para*-phenylene ethynylene)s with thioacetyl end groups (TA-PPE).^[176] These solution-processed OPTs show $R = 36 \text{ mA/W}$ and $I_{ph}/I_{dark} = 3.3 \times 10^3$ at $V_g = 0 \text{ V}$. The applied gate bias of the OPTs presumably provided an efficient route for the dissociation of the photo-generated excitons into free electrons and holes.

It was considered that increasing the light intensity is a typical way to enhance the photocurrent in OPTs. However, Wasapinyokul et al. found that the rate of photoinduced current in poly(3,3'''-didodecylquarter-thiophene) (PQT-12)-based OPTs was increased while increasing the light intensity only in a limited range, eventually reaching a maximum

before decreasing.^[177] This phenomenon was explained in terms of photogenerated polarons recombination occurring at high photocarrier densities. When at high light intensity the polaron density exceeds a threshold value of $1.6\text{--}2.2 \times 10^{17} \text{ cm}^{-3}$, the number of polarons cannot increase further as they are already closely packed and recombination overtakes generation, resulting in a decrease of I_d from its peak value.^[140]

5.2.1. Blended Polymer Semiconductors

Donor-acceptor blends that are typically used for organic photovoltaic devices can be envisioned as an active layer for fast response OPTs. Anthopoulos demonstrated an ambipolar OPT device and electro-optical organic circuits using blends of [66]-phenyl-C₆₁-butyric acid methyl ester (PC₆₁BM) and poly (2-methoxy-5-(3',7'-dimethyloxy-*p*-phenylene vinylene) (OC₁C₁₀PPV). Interestingly, the blended-ambipolar OPT exhibited very fast total response time of $\sim 65 \mu\text{s}$ (corresponding to an operation frequency of $\sim 15 \text{ kHz}$), which is much faster than typical unipolar OPTs (typically above a few tens of ms). This can be attributed to the efficient photo-generation of excitons in OC₁C₁₀PPV and fast charge separation into free electrons and holes at the interface of PC₆₁BM:OC₁C₁₀PPV. By carefully tuning the ambipolar charge transport character of the

PC₆₁BM:OC₁C₁₀PPV-blended OPTs, their photoresponsivity can be controlled and optimized, and consequently applied to a variety of electro-optical switches and logic circuits, such as NOT and OR gates (Figure 13).^[178] Such optoelectronic circuits can potentially be applied in electro-optical transceivers and full-color image sensor arrays.

Mok et al. introduced light sensitive OPTs using a composite of P3HT and TiO₂ nanoparticles.^[179,180] These devices showed relatively fast response ($\sim 0.2 \text{ s}$) under light exposure, exhibiting a maximum light absorbance at 520 nm. The photogeneration mechanism is attributed to photons absorbed by P3HT, generating excitons which are effectively separated into charges at the P3HT-TiO₂ interface, as shown in Figure 14. Accumulated electrons that are trapped in the TiO₂ nanoparticles (NPs) (which have a LUMO of -4.3 eV to be compared with LUMO of P3HT of -3.2 eV), increase the potential of the channel owing to a floating body effect in the transistor, and therefore induce a positive V_{Th} shift, while not evidently affecting field-effect mobility, off current, and subthreshold slope. The photosensitivity of this OPT device has been found to be dependent on the concentration of TiO₂ NPs, the incident light wavelength, and V_d .^[179] In contrast to previous report on bulk heterojunction OPTs with MDMO-PPV:PC₆₁BM, TiO₂ NPs do not form continuous channel so there is no contribution of electrons to the channel current under light illumination. The non-linear behavior with light intensity can be attributed either to built-

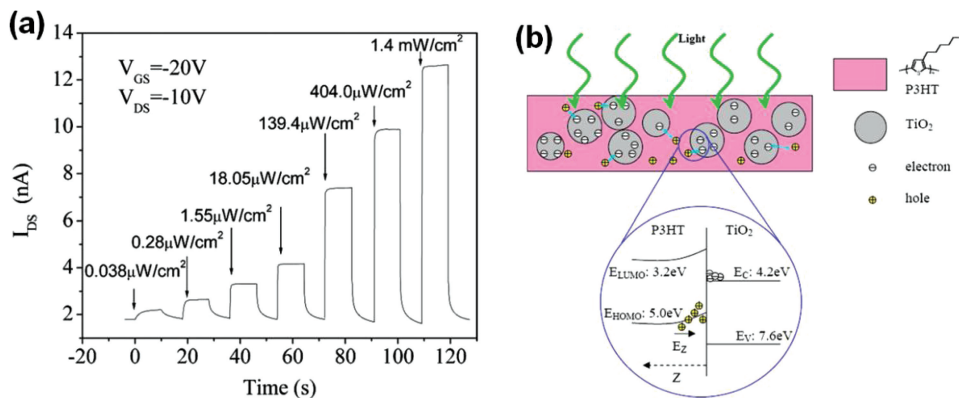


Figure 14. (a) The channel current of an OPT based on a composite of P3HT and TiO₂ NPs measured under light illumination (UV, $\lambda = 370\text{ nm}$) with different intensities. Weight ratio of P3HT:TiO₂ = 1: 0.75; average grain size of TiO₂ (rutile): 5 nm \times 20 nm. (b) Schematic diagram showing charge accumulation in a P3HT/TiO₂ composite film under light illumination. Reproduced with permission from Ref. [180]. Copyright 2009, American Institute of Physics.

in potential and retarded charge transfer due to accumulated electrons at the interface between P3HT and discrete TiO₂ NPs, or to the occurrence of the exciton-exciton annihilation within P3HT layer at higher light intensity which results in decreased exciton lifetime. The separation of excitons into charges can be enhanced by the application of an external electric field.^[142]

The photo-sensitive properties of polymer macromolecules can be modified by employing dye-doping thus developing wavelength-selective field-effect phototransistors. The dye-doped P3HT OPTs with coumarin 6 (C6), oxazine 1, and nile red, resulted in tuning the wavelength sensitivity in the range from 400 nm to 700 nm depending on the particular dye.^[181] Transconductance (g_m) of the C6-doped P3HT OPTs increased from $g_m = 1.3\text{ pA/V}$ to 460 pA/V (at $V_g = -10\text{ V}$ and $V_d = -30\text{ V}$) when irradiated at 440 nm with an intensity of 2.4 mW/cm². This increase in the transistor current under illumination was attributed to an enhanced photoconductivity of the accumulation layer at the semiconductor-dielectric interface owing to the additional light absorption of the dye molecules. Consequently, there is a strong

correlation between the absorption in the solid state and the spectral response of the phototransistor based on the dye-doped semiconductors. Figures of merits of most relevant polymeric OPTs are reported in Table 4.

6. Applications of Organic Photodetectors

6.1. Integrated Transceivers

One of the very interesting advantages of OPDs is that they lend themselves to be easily integrated with other optical components, providing cost-effective building blocks for alternative integrated electro-optical circuits as well as lab-on-chip components.^[182] OPDs have been directly fabricated for example on waveguides.^[183,184] The combination of OPDs with OLEDs and polymeric elements makes it possible to realize flexible integrated components for electro-optical transceivers.

Table 4. OPTs based on Polymer semiconductors.

	Semiconductor	Structure (Dielectric)	Mobility [$\text{cm}^2/\text{V}\cdot\text{s}$]	Responsivity (Light source, Intensity)	$I_{d,\text{ph}}/I_{d,\text{dark}}$	$t_R^{\text{a)}$	Ref.
Single Layer	P3OT	BG/TC (PVA)	$10^{-3}\text{--}10^{-4}$	1 A/W (532 nm, 1 mW/cm ²)	$10^2\text{--}10^3$	NA	[169]
	P3HT	BG/TC (PVA)	2.6×10^{-3}	NA (1 mW/cm ²)	NA	< 20 ms	[212]
		BG/BC (SiO ₂)	0.01–0.07	245 (White light, 51 mW/cm ²)	3.8×10^3	NA	[213]
	PQT-12	TG/BC (PMMA/PVP)	1.1×10^{-3}	6.6 A/W (525 nm, 3 $\mu\text{W}/\text{cm}^2$)	$\sim 10^2$	NA	[177]
	F8T2	BG/TC (BCB/SiN _x)	3×10^{-3}	0.7 mA/W \sim 1 A/W (White light, 2.9 mW/cm ²)	10^3	NA	[173,172]
		BG/BC (SiO ₂)	1.2×10^{-4}	18.5 A/W (465 nm, 5 $\mu\text{W}/\text{cm}^2$)	$\sim 10^2$	NA	[174]
	BAS-PPE	BG/BC (Polyimide)	NA	5 mA/W (White light, 4 $\mu\text{W}/\text{cm}^2$)	6000	NA	[175]
	TA-PPE	BG/TC (SiO ₂)	NA	0.036 A/W (5.76 mW/cm ²)	3.3×10^3	NA	[176]
	MDMO-PPV:PC ₆₁ BM	BG/BC (SiO ₂ , HMDS)	$10^{-4}\text{--}10^{-3}$	NA (469 nm)	10^4	$\sim 16\text{ }\mu\text{s}$	[178]
	P3HT:Dye	BG/BC (SiO ₂)	NA	NA	NA	NA	[181]
Blends	P3HT:TiO ₂	BG/BC (SiO ₂)	NA	NA (370 \sim 590 nm, 0.2 mW/cm ²)	$\sim 10^3$	$\sim 0.2\text{ s}$	[179,180]

^{a)} t_R is the device response time.

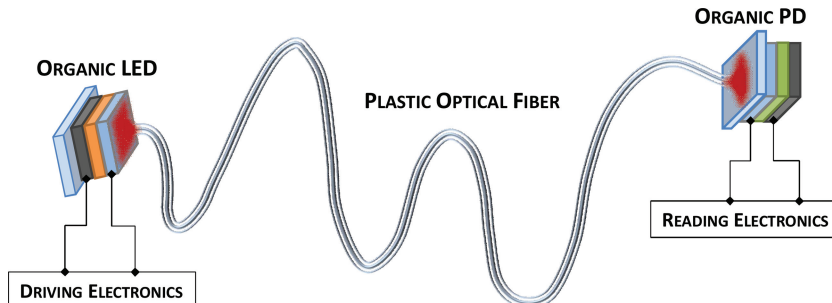


Figure 15. Schematic drawing of an optical data link comprising an OLED transmitter and an OPD receiver, connected through a POF.

Vacuum deposited OPDs based on multilayers of donor and acceptor phthalocyanine derivatives, with a cut-off frequency of 5 MHz at an applied bias of 4 V, were fabricated on polymeric waveguides.^[184] This receiver, optimized to work in the red region at 640 nm, was connected through an optical fiber to an OLED transmitter, which was fabricated as well on a polymeric waveguide, realizing an electro-optical integrated system.

This concept was further elaborated to demonstrate an optical data link capable to transmit a standardized protocol by making use of organic components only (**Figure 15**).^[185] A vacuum processed OLED with an emission peak at 520 nm was simply butt-coupled to a poly(methyl methacrylate) (PMMA)-based plastic optical fiber (POF), which shows low attenuation around 500 nm.^[186] On the other side the POF is coupled to the glass substrate of a solution-processed OPD based on a P3HT:PC₆₁BM bulk-heterojunction, which is well matched to the peak emission of the OLED. When reverse biased at 5 V, the OPD adopted in this system showed a spectral responsivity of 0.24 A/W and a 90%–10% fall time of 40 ns, a time response which is good enough for the Sony/Philips Digital Interface Format standard (S/PDIF). With this system a S/PDIF digitized audio signal was successfully transmitted at bit rate of 2.8224 Mbit/s. Though coupling of a POF with a detector is simpler than for standard optical fibers due to rather large cores and high numerical apertures, losses are inevitable. A radical solution to this issue was proposed, where a solution processed OPD is directly fabricated on the cutting edge of a POF.^[187]

6.2. Imaging Applications

Digital imaging is another broad and interesting field of applications where OPD could allow the development of revolutionary devices characterized by large-area, ruggedness, light-weight, flexibility and low-cost. Conformable devices mimicking the human eye and flexible digital X-ray detectors represent clear examples where OPD imagers could make a difference. We can distinguish here passive and active matrix devices. In a *passive matrix*, OPDs are simply assembled in a cross-bar array. This architecture is very

simple, but it poses severe readout problems and it is susceptible to pixel-to-pixel cross-talk due to the absence of pixel selectors. In particular only small arrays are possible, since the dark current, which is proportional to overall size, increases with increasing number of lines. One of the most remarkable demonstrations where a passive matrix of OPDs was adopted regards a hemispherical focal plane detector array. Here a preformed plastic substrate with a 1 cm radius is adopted in order to mimic the curvature and function of the human eye, where the nearly spherical shape allows focusing through a single lens element (**Figure 16**).^[188] Vacuum processed, bilayer OPDs based on a copper phthalocyanine and C₆₀ fullerene were defined between patterned Au anode and Ag cathode. The key point in demonstrating the hemispherical focal plane was the adoption of a transfer technique based on elastomeric stamps where metals are cold welded on preformed strike layers, thus allowing formation of unstrained metallic cross-bars. Up to 100 × 100, (40 μm)² pixels were defined without failure, where OPDs showed a spectral responsivity of 65 mA/W with D* = 5 × 10¹⁰ cmHz^{1/2}/W and a 90%–10% fall time of less than 100 ns.

Active matrix solutions are more suitable for large area applications. Here the OPD is integrated with one or more transistors, which, depending on the chosen architecture, can act as simple selectors or can also integrate part of the readout. The most simple pixel architecture is based on the so called *passive pixel*, formed by one detector and one transistor acting as row selector (**Figure 17**). Passive pixels based on an OPD were fabricated both in a vertically stacked and in a co-planar integrated

architecture. A vacuum processed, integrated passive pixel was recently demonstrated by the group of S. R. Forrest, both in a configuration comprising a bottom gate, bottom contacts pentacene FET and a bottom-illuminated subphthalocyanine (SubPc)/C₆₀ vertical OPD,^[189] and in the case of a bottom gate, top contacts FET and a top-illuminated OPD, fabricated with the same active materials (**Figure 18**).^[190] In the second case the superior performance of the staggered OFET architecture in terms of field-effect mobility^[138] allows a higher dynamic range, therefore a more extended linear response of the photocurrent vs. incident power density. Top illumination is feasible thanks to an inverted OPD structure, where a transparent

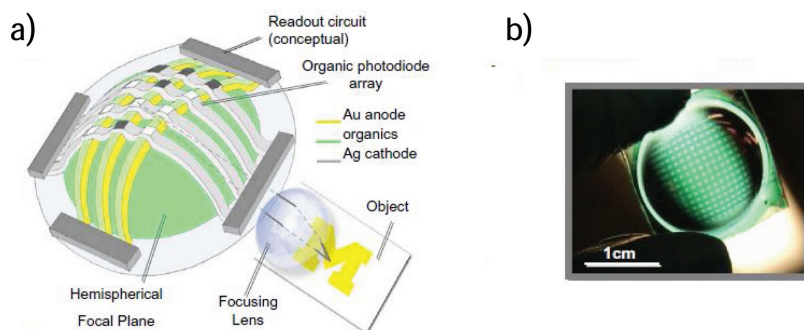


Figure 16. Scheme (a) and photograph (b) of the hemispherical focal plane array based on a passive matrix of OPDs. In the scheme the integration in a hypothetical imaging system is depicted. The photograph shows the 11 × 13 array of 500 μm × 500 μm detectors fabricated on a 1 cm radius plastic substrate. Adapted from Ref. [188]. Copyright 2008, Elsevier B.V.

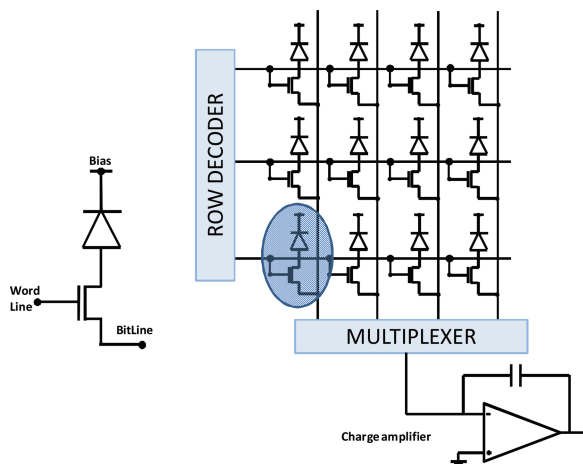


Figure 17. Schematic drawing of a passive pixel (on the left), composed of a detector connected to a FET acting as a switching element, and of a simple 3×4 array (on the right) based on this architecture. In the array additional circuitry is needed for correct pixel addressing and readout: a row decoder drives the word (gate) lines and a multiplexer scans the columns to connect the pixel to the common readout circuit.

ITO top contact is sputtered on top of MoO_3 interlayer. At -2 V bias the pixel responsivity is about 80 mA/W at 580 nm , with a lowest detectable intensity of $17\text{ }\mu\text{W/cm}^2$ and with a specific detectivity of $9.4 \times 10^{11}\text{ cmHz}^{1/2}/\text{W}$. The read-out time is 0.4 ms , limited by the discharging time through the OFET. This pixel is overall suitable for video-rate detection and could be integrated in arrays up to 30×30 pixels.

Vertically stacked passive pixels, where the transistor is integrated beneath the OPD active area, could represent a very interesting alternative since they would allow to achieve a higher geometrical fill-factor (FF, defined as the ratio between the active detector area and the overall pixel area),^[191] though increasing the number of stacked layers and therefore complicating the fabrication process. In vertical passive pixels, the transistor is fabricated first and then passivated in order to protect it during the detector processing. A vertical interconnection is also required between the transistor source/drain

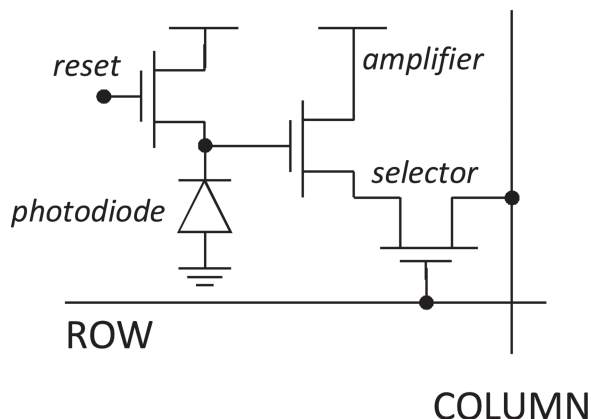


Figure 19. Schematic of an active pixel architecture.

pad and the detector. This kind of architecture was adopted to fabricate wavelength selective hybrid pixels based on organic detectors and a ZnO TFT.^[192] Green and red sensitive photodetectors were adopted, where NN -dimethylquinacridone and 2,9-di(pyrid-2-yl)-anthra[2,1,9-def:6,5,10-d'e'f]diisoquinoline-1,3,8,10-tetrone, with electron and hole transport properties respectively, were used for the green detector, while zinc phthalocyanine and titanyl phthalocyanine were used for the red detector. The two pixels, with photoresponsivity peak at 540 nm and 700 nm respectively, were simply stacked one on top of the other, in order to realize a pixel capable of discriminating colors. This was the base for realizing a 47×30 pixels image sensor, with a $600\text{ }\mu\text{m}$ pitch, capable of TV frame rate response. Though being limited in this case to two colors, if suitably extended this may represent an interesting prism-less/filter-less alternative for future color cameras.

An *active pixel* instead is a more complicated architecture where at least three transistors are integrated with the detector to provide both the selecting and signal amplification capability to the pixel.^[193] This is a robust and promising approach, though more complicated and possibly characterized by a lower geometrical FF compared to a passive architecture because of the space needed to accommodate the additional transistors. This concept was applied to an OPD in combination with amorphous silicon thin-film transistors (TFTs) to give an hybrid active pixel (Figure 19).^[193] In order to obtain a FF close to 100%, a stacked architecture was adopted: firstly the transistors back-plane is fabricated and then a bulk-heterojunction P3HT:PC₆₁BM OPD array is integrated on top. The bottom gold electrode of the OPD is connected to the gate of the amplifying transistor, whose transconductance directly affects the charge amplification gain. It was demonstrated that the smallest detectable signal with such active pixel can be as low as $1\text{ }\mu\text{W/cm}^2$ at 522 nm , compared to a value of $6\text{ }\mu\text{W/cm}^2$ obtained with a passive pixel fabricated with the same technology, thanks to the charge amplification integrated in the pixel.

There are a few other impressive OPD based active-matrix imagers presented in the literature so far, mainly based on the passive pixel architecture. Among hybrid organic-inorganic examples, Street and collaborators demonstrated a flexible sensor array, where a non-patterned organic layer of the

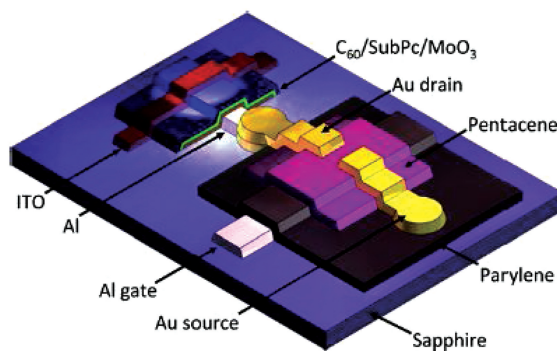


Figure 18. Scheme of an integrated passive pixel where an inverted $\text{C}_{60}/\text{SubPc}$ OPD is laterally integrated with a bottom-gate, top-contact pentacene OFET. Reproduced with permission from Ref. [190]. Copyright 2011, Elsevier B.V.

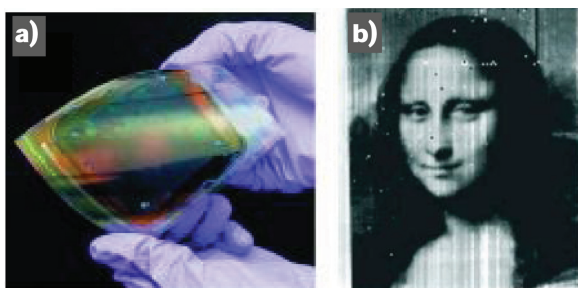


Figure 20. (a) An imager based on OPDs and a:Si backplane, fabricated at low temperature on a flexible polyester substrate; (b) an approximately 5 cm x 3.8 cm image obtained with the flexible imager. Adapted with permission from Ref. [61]. Copyright 2008, American Institute of Physics.

photoactive blend poly[2-methoxy-5-(2-ethylhexyloxy)-1,4-phenylene-vinylene] (MEH-PPV) and PC₆₁BM was deposited on top of a flexible amorphous silicon TFT backplane with 180 × 180 pixels, with a 75 dots per inch resolution, fabricated by inkjet digital lithography on a polyethylene naphthalate (PEN) substrate (**Figure 20**).^[61] To provide light access in this case the top-electrode was formed by spin-coating an ITO nano-particles dispersion. The pixel FF was 0.76. As already reported in Section 4.2, dark currents lower than 1 nA/cm² at an applied bias voltage of -4 V, comparable to what is achievable with standard silicon *p-i-n* photodiodes, were achieved by adopting a very thick blend layer of 4 μm. The EQE of the integrated detector was 35% at 488 nm, with a NEP of 30 pW/cm² with an integration time of 100 ms. The sensor response time allows images detection with a frame rate of 500 Hz.

A very remarkable demonstration for NIR imaging in the case of hybrid technologies was achieved by adopting solution processed, quantum-dot sensitized P3HT:PC₆₁BM detectors^[104] integrated with an amorphous silicon TFT backplane (**Figure 21**). The ternary blend sensitizes the OPD in the 1 to 2 μm range, where nanocrystalline PbS quantum-dots act as antennas and exciton dissociation leads to the formation of a hole which is transferred to P3HT and an electron, transferred to PC₆₁BM. EQE up to ~50% was demonstrated at a reverse bias of 8 V. The photoactive film was unpatterned, while the active matrix backplane was formed by 256 × 256 pixels with a 154 μm pitch, with a FF = 83.3%. A specific detectivity *D** of 2.3 ×

10⁹ cmHz^{1/2}/W was obtained, with a -3 dB frequency of 2.5 kHz, limited by the parasitic capacitance of the TFT and compatible with imaging applications with tens of Hz frame rates.

Very recently, an hybrid complementary metal oxide semiconductor-imager was reported as well, where a P3HT:PCBM detector replaced a Si photodiode, therefore enabling the achievement of a geometrical fill-factor close to 100%.^[194]

There are also examples in the literature where the sensor arrays were fabricated based on an all-organic passive pixel, where both the detector and transistor are based on organic semiconductors. A proof-of-concept 4 × 4 active-matrix was demonstrated based on a passive pixel fabricated by standard photolithography combined with inkjet printing.^[195] A lateral photodetector based on a tytanil phthalocyanine was laterally integrated next to a bottom-gate, bottom-contact pentacene FET. The lateral geometry of the detector allows easy access of the light and easy integration of the photoactive material by inkjet printing as the last step of the process. In this proof-of-concept the pixel responsivity at 530 nm was limited to 6 × 10⁻⁵ A/W at a luminance of 5 mW/cm², which is anyway enough to correctly image a "T" pattern after a proper first-order calibration.

Another application of an all-organic passive pixel array was proposed, where an array of pixels with 36 dpi resolution was created on a PEN foil and operated as a sheet image scanner.^[19] In this case the OPD, a D/A bilayer based on phthalocyanine and perylene derivatives, and OFET, based on pentacene, were vacuum processed separately and only successively integrated by lamination. The working mechanism is based on the possibility to distinguish black from white parts on paper thanks to their different reflectivity, OPDs being shielded from direct light and exposed only to reflected light. The proposed scanning solution does not require optics and mechanical parts.

6.3. Other Applications

There are many other applications where OPD can be integrated and successfully adopted. For example position sensors have been proposed, based on different working mechanism. One of these *position-sensitive* OPDs was based on a 3-cm long double-layer, vacuum processed detector, where the resistive ITO anode offered the possibility to detect a beam position with 20 μm accuracy. The position can be simply detected by exploiting a

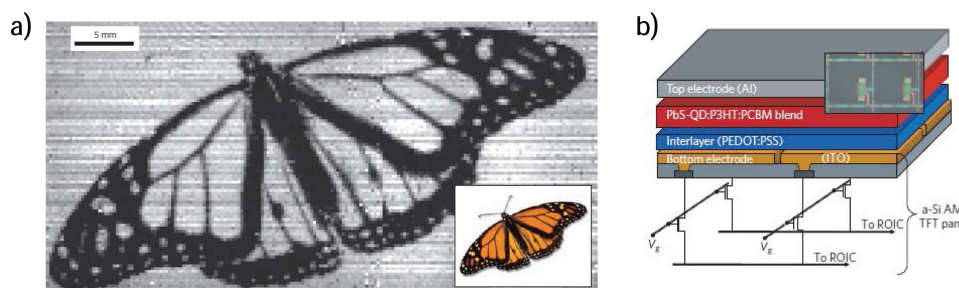


Figure 21. a) 1310 nm image of a butterfly obtained with a quantum-dot sensitized NIR OPD imager. b) Schematic view of the imager, where the quantum-dot sensitized OPDs are integrated on top of a a:Si backplane: the pixel area is defined by the patterned ITO bottom contact connected to its corresponding switch, while the photoactive blend is not patterned. Adapted with permission from Ref. [104]. Copyright 2009, Macmillan Publishers Limited.

voltage divider while reading both currents at the two lateral edges of the resistive anode.^[196] The device was demonstrated to be capable of tracking signals up to 2 m/s in the 550 to 700 nm range. Another approach to realize a position sensor was recently demonstrated with a proof-of-concept device based on a bilayer D/A with complementary lateral thickness gradient.^[197] The spectral response of such device varies along the lateral direction due to a gradual variation from an acceptor C₆₀ rich area to a donor CuPc rich area. The ratio of photoresponse at two different wavelengths allows position detection with a 600 μm accuracy already in a non-optimized device.

Recently organic photosensors for *high-luminance detection* were proposed as well, where, very interestingly, an all inkjet printed OPD with an inverted structure was adopted.^[198] A silver electrode was printed to form the opaque cathode, on top of which a thick blend based on electron accepting poly(9,90-diptylfluorene-co-benzo-thiadiazole) (F8BT) and electron donor poly(9,90-diptylfluorene-co-bis-N,N-(4-butylphenyl)-bis-N,N-phenyl-1,4-phenylenediamine) (PFB) was printed as well. A thickness of approximately 1 μm of the blend was necessary to reduce dark currents. A transparent PEDOT:PSS anode was printed on hydrophobic blend by adding a surfactant to the conductor formulation. The detector was showed to be capable of linearly responding to high luminance fluxes of 100–400 klux.

7. Conclusions

Organic light signal detectors are devices with strong potential for being cost-effectively adopted in a variety of applications such as short-range data transmission, digital imaging and sensing. They are characterized by easy tunability, integrability, and by the possibility to achieve wavelength selectivity. The ease of processing, the vast library of materials and properties, and the high quantum yield and responsivity achieved thanks to donor-acceptor heterojunctions allow to envision a widespread adoption of these detectors, provided that minimum requisites regarding reliability and long-term stability are met.

Here we presented a review of working mechanisms, recent progress and applications of the most widely adopted architecture of organic detectors: photodiodes and phototransistors.

Organic photodiodes have reached a mature level, benefiting from the steady development of efficient photoconverting materials for organic photovoltaics, which allows to easily reach (at least in the peak of absorbance of a specific materialblend) EQE > 80% in the visible or NIR, corresponding to responsivities in the 0.1–0.5 A/W range. Differently from solar cells, in detectors an external electric field can be applied to optimize charge generation and collection (i.e. quantum efficiency and response time), paying attention to limit the amount of injected charges from the electrodes (i.e. the dark current), strongly contributing to the noise and therefore limiting the device detectivity. Suitable architectures allow to reach dark currents <1 nA/cm², a value comparable to what can be achieved in p-i-n Si photodiodes. Overall specific detectivities D^* of many 10¹² (cm Hz^{0.5})/W can be obtained. Regarding the response time, fast detectors capable of operating at frequencies higher than 100 MHz are possible thanks to multilayered structures, while in bilayered vacuum evaporated devices the range is usually between

10 and 100 MHz. Solution-processed bulk heterojunctions show a trade-off between ease of processing and operation frequency, which was possible to push to >1 MHz in various cases. Within this very promising scenario, it must be noted though that the simultaneous optimization of EQE, bandwidth and detectivity is demonstrated in a limited number of publications only, and a sizeable number of them fails to characterize the response speed and/or the dark current magnitude, while all these three parameters are really qualifying figures of merit for photodiodes.

Phototransistors, organic photodetectors based on OFETs structure, are a type of optical transducer in which light detection and signal amplification are combined in a single device. OPTs showed two different responses as the result of photo-illumination, i.e., photoconductive (transistor in off state) and photovoltaic effects (transistor in on state). To obtain high performance OPTs, the OFET must show good device characteristics with a high mobility in the absence of irradiation of light. The most efficient OPT device exhibited a photo-responsivity of more than 12000 A/W, which is much higher value than that of amorphous silicon-based PTs of ~300 A/W.

Acknowledgements

Y. Y. acknowledges financial support from a grant (code No. 2012-054547) from the Center for Advanced Soft Electronics under the Global Frontier Research Program of the Ministry of Education, Science and Technology, Korea and a grant from the Basic Science Research Program through the National Research Foundation of Korea (NRF), funded by the Ministry of Education, Science and Technology (MEST) (2010-0023180). M. B. and D. N. gratefully acknowledge M. Sampietro for strongly supporting the activity and A. Iacchetti for fruitful discussions. M. C., M. B. and D. N. acknowledge partial support from Fondazione Cariplo for funding under project Indixi, Grant n. 2011-0368. M. C. acknowledges EU partial support through the Marie-Curie Career Integration Grant "IPPIA", within the European Union Seventh Framework Programme (FP7/2007-2013) under grant agreement n° PCIG09-GA-2011-291844.

Received: December 4, 2012

Published online: March 11, 2013

Note: Figure 5 was replaced after initial online publication.

- [1] H. Dong, H. Zhu, Q. Meng, X. Gong, W. Hu, *Chem. Soc. Rev.* **2012**, *41*, 1754.
- [2] G. C. Schmidt, M. Bellmann, H. Kempa, M. Hambsch, K. Reuter, M. Stanel, A. C. Hübner, *MRS Online Proceedings Library* **2011**, 1285.
- [3] N. T. Kalyani, S. J. Dhoble, *Rnew. Sust. Energ. Rev.* **2012**, *16*, 2696.
- [4] H. Sirringhaus, P. IEEE **2009**, *97*, 1570.
- [5] Y. Lin, Y. Li, X. Zhan, *Chem. Soc. Rev.* **2012**, *41*, 4245.
- [6] J. Nelson, *Mater. Today* **2011**, *14*, 462.
- [7] B. Cho, S. Song, Y. Ji, T.-W. Kim, T. Lee, *Adv. Funct. Mater.* **2011**, *21*, 2806.
- [8] M. D. Angione, R. Pilolli, S. Cotrone, M. Magliulo, A. Mallardi, G. Palazzo, L. Sabbatini, D. Fine, A. Dodabalapur, N. Cioffi, L. Torsi, *Mater. Today* **2011**, *14*, 424.
- [9] D. Briand, A. Oprea, J. Courbat, N. Bârsan, *Mater. Today* **2011**, *14*, 416.
- [10] B. Lucas, T. Trigaud, C. Videlot-Ackermann, *Polym. Int.* **2012**, *61*, 374.
- [11] B. Kippelen, J.-L. Bredas, *Energy Environ. Sci.* **2009**, *2*, 251.

- [12] J. Cabanillas-Gonzalez, G. Grancini, G. Lanzani, *Adv. Mater.* **2011**, *23*, 5468.
- [13] I. G. Scheblykin, A. Yartsev, T. Pullerits, V. Gulbinas, V. Sundström, *J. Phys. Chem. B* **2007**, *111*, 6303.
- [14] N. Geacintov, M. Pope, *J. Chem. Phys.* **1967**, *47*, 1194.
- [15] V. I. Arkhipov, E. V. Emelianova, H. Bässler, *Phys. Rev. Lett.* **1999**, *82*, 1321.
- [16] H. Najafov, B. Lyu, I. Biaggio, V. Podzorov, *Phys. Rev. B* **2008**, *77*, 125202.
- [17] More complicated phenomena can take place at the D/A interface, such as: energy transfer from D(A) to A(D) followed by hole(electron) transfer to D(A); energy transfer followed by inter-system crossing etc.
- [18] G. Yu, A. J. Heeger, *J. Appl. Phys.* **1995**, *78*, 4510.
- [19] T. Someya, Y. Kato, I. Shingo, Y. Noguchi, T. Sekitani, H. Kawaguchi, T. Sakurai, *IEEE T. Electron Dev.* **2005**, *52*, 2502.
- [20] M. A. Ruderer, P. Muller-Buschbaum, *Soft Matter* **2011**, *7*, 5482.
- [21] M. A. Brady, G. M. Su, M. L. Chabinyc, *Soft Matter* **2011**, *7*, 11065.
- [22] D. Beljonne, J. Cornil, L. Muccioli, C. Zannoni, J. L. Bredas, F. Castet, *Chem. Mater.* **2011**, *23*, 591.
- [23] F. Laquai, Y.-S. Park, J.-J. Kim, T. Basché, *Macromol. Rapid Commun.* **2009**, *30*, 1203.
- [24] C. Deibel, T. Strobel, V. Dyakonov, *Adv. Mater.* **2010**, *22*, 4097.
- [25] V. I. Arkhipov, P. Heremans, H. Bassler, *Appl. Phys. Lett.* **2003**, *82*, 4605.
- [26] S. Verlaak, P. Heremans, *Phys. Rev. B* **2007**, *75*, 115127.
- [27] T. M. Clarke, J. R. Durrant, *Chem. Rev.* **2010**, *110*, 6736.
- [28] G. Grancini, M. Maiuri, D. Fazzi, A. Petrozza, H.-J. Egelhaaf, D. Brida, G. Cerullo, G. Lanzani, *Nat. Mater.* **2013**, *12*, 29.
- [29] A. C. Morteani, P. Sreearunothai, L. M. Herz, R. H. Friend, C. Silva, *Phys. Rev. Lett.* **2004**, *92*, 247402.
- [30] Sizeable relaxation always occurs in organic molecules upon changing their oxidation state, as it is the case for charge transfer. Generally speaking, electron transfer has to take place isomerically, hence it proceeds when, thanks to vibrational motion, a configuration is reached so that for an electron it is energetically equivalent to reside on the A moiety (D^+A^- state, reactant) or on the D moiety (DA state, product). The energy to reach such a configuration is the activation energy for the reaction, which turns out to be equal to $(\Delta G_0 + \lambda)^2 / 4\lambda$, where ΔG_0 is the free energy of the reaction (neglecting entropy it is the energy difference between thermalized products and reactants), and λ is the reorganization energy (which is the energy needed to bring the reactant and its surrounding medium to the equilibrium geometry of the products). While the transfer rate is maximized when $\Delta G_0 = \lambda$, for $-\Delta G_0$ increasingly larger than λ the rate is lowered because, despite the fact that the reaction becomes more exergonic, the configuration of isoenergetic electron transfer is reached with a larger distortion of reactant geometry, thus requiring a larger activation energy.
- [31] C. W. Schlenker, V. S. Barlier, S. W. Chin, M. T. Whited, R. E. McAnally, S. R. Forrest, M. E. Thompson, *Chem. Mater.* **2011**, *23*, 4132.
- [32] T. Agostinelli, M. Caironi, D. Natali, M. Sampietro, P. Biagioni, M. Finazzi, L. Duo, *J. Appl. Phys.* **2007**, *101*, 114504.
- [33] R. H. Bube, *Photoconductivity of solids*, John Wiley & Sons, Inc., New York **1960**.
- [34] G. Horowitz, *J. Mater. Res.* **2004**, *19*, 1946.
- [35] Due to the small electric field over L-L', carriers spend enough time there to undergo recombination.
- [36] M. A. Lampert, P. Mark, *Current Injection in Solids*, Academic Press, New York **1970**.
- [37] A. M. Goodman, A. Rose, *J. Appl. Phys.* **1971**, *42*, 2823.
- [38] V. D. Mihailescu, J. Wilderman, P.W. M. Blom, *Phys. Rev. Lett.* **2005**, *94*, 126602.
- [39] L. Tzabari, N. Tessler, *J. Appl. Phys.* **2011**, *109*, 064501.
- [40] T. Kirchartz, B. E. Pieters, J. Kirkpatrick, U. Rau, J. Nelson, *Phys. Rev. B* **2011**, *83*, 115209.
- [41] R. A. Street, *Phys. Rev. B* **2011**, *84*, 075208.
- [42] A. Iacchetti, D. Natali, M. Binda, L. Beverina, M. Sampietro, *Appl. Phys. Lett.* **2012**, *101*.
- [43] M. A. Romero, M. A. G. Martinez, P. R. Herczfeld, *IEEE Trans. Microwave Theory Tech.* **1996**, *44*, 2279.
- [44] A. J. Seeds, A.A. A. Desalles, *IEEE Trans. Microwave Theory Tech.* **1990**, *38*, 577.
- [45] C. S. Choi, H. S. Kang, W. Y. Choi, H. J. Kim, W. J. Choi, D. H. Kim, K. C. Jang, K. S. Seo, *IEEE Photonics Technol. Lett.* **2003**, *15*, 846.
- [46] H. S. Kang, C. S. Choi, W. Y. Choi, D. H. Kim, K. S. Seo, *Appl. Phys. Lett.* **2004**, *84*, 3780.
- [47] Y. F. Xu, P. R. Berger, J. N. Wilson, U. H. F. Bunz, *Appl. Phys. Lett.* **2004**, *85*, 4219.
- [48] B. Lucas, T. Trigauda, C. Videlot-Ackermann, *Polym. Int.* **2011**, *61*, 374.
- [49] S. M. Sze, K. K. Ng, *Physics of Semiconductor Devices*, Wiley-Interscience, New Jersey **2007**.
- [50] Q. Chen, T. Hajagos, Q. Pei, *Annual Reports Section "C" (Physical Chemistry)* **2011**, *107*, 298.
- [51] M. Binda, D. Natali, M. Sampietro, T. Agostinelli, L. Beverina, *Nucl. Instrum. Meth. A* **2010**, *624*, 443.
- [52] B. Fraboni, A. Ciavatti, F. Merlo, L. Pasquini, A. Cavallini, A. Quaranta, A. Bonfiglio, A. Fraleoni-Morgera, *Adv. Mater.* **2012**, *24*, 2289.
- [53] A. Iacchetti, M. Binda, D. Natali, M. Giussani, L. Beverina, C. Fiorini, R. Peloso, M. Sampietro, *IEEE T. Nucl. Sci.* **2012**, *59*, 1862.
- [54] N. S. Sariciftci, D. Braun, C. Zhang, V. I. Srdanov, A. J. Heeger, G. Stucky, F. Wudl, *Appl. Phys. Lett.* **1993**, *62*, 585.
- [55] J. J. M. Halls, C. A. Walsh, N. C. Greenham, E. A. Marseglia, R. H. Friend, S. C. Moratti, A. B. Holmes, *Nature* **1995**, *376*, 498.
- [56] G. Yu, Y. Cao, J. Wang, J. McElvain, A. J. Heeger, *Synth. Met.* **1999**, *102*, 904.
- [57] P. Peumans, V. Bulovic, S. R. Forrest, *Appl. Phys. Lett.* **2000**, *76*, 2650.
- [58] M. Ramuz, L. Bürgi, C. Winnewisser, P. Seitz, *Org. Electron.* **2008**, *9*, 369.
- [59] S. F. Tedde, J. Kern, T. Sterzl, J. Furst, P. Lugli, O. Hayden, *Nano Lett.* **2009**, *9*, 980.
- [60] K. S. Nalwa, Y. Cai, A. L. Thoeming, J. Shinar, R. Shinar, S. Chaudhary, *Adv. Mater.* **2010**, *22*, 4157.
- [61] T. N. Ng, W. S. Wong, M. L. Chabinyc, S. Sambandan, R. A. Street, *Appl. Phys. Lett.* **2008**, *92*, 213303.
- [62] A. C. Niemeyer, I. H. Campbell, F. So, B. K. Crone, *Appl. Phys. Lett.* **2007**, *91*, 103504.
- [63] F. Zhang, M. Johansson, M. R. Andersson, J. C. Hummelen, O. Inganäs, *Adv. Mater.* **2002**, *14*, 662.
- [64] J. K. J. van Duren, X. Yang, J. Loos, C. W. T. Bulle-Lieuwma, A. B. Sieval, J. C. Hummelen, R. A. J. Janssen, *Adv. Funct. Mater.* **2004**, *14*, 425.
- [65] M. M. Wienk, J. M. Kroon, W. J. H. Verhees, J. Knol, J. C. Hummelen, P. A. van Hal, R. A. J. Janssen, *Angew. Chem. Int. Ed.* **2003**, *42*, 3371.
- [66] T. Hamasaki, T. Morimune, H. Kajii, S. Minakata, R. Tsuruoka, T. Nagamachi, Y. Ohmori, *Thin Solid Films* **2009**, *518*, 548.
- [67] P. E. Keivanidis, S.-H. Khong, P. K. H. Ho, N. C. Greenham, R. H. Friend, *Appl. Phys. Lett.* **2009**, *94*, 173303.
- [68] B. Friedel, P. E. Keivanidis, T. J. K. Brenner, A. Abrusci, C. R. McNeill, R. H. Friend, N. C. Greenham, *Macromolecules* **2009**, *42*, 6741.
- [69] P. E. Keivanidis, P. K. H. Ho, R. H. Friend, N. C. Greenham, *Adv. Funct. Mater.* **2010**, *20*, 3895.

- [70] A. Kobayashi, M. Sasa, W. Suzuki, E. Fujiwara, H. Tanaka, M. Tokumoto, Y. Okano, H. Fujiwara, H. Kobayashi, *J. Am. Chem. Soc.* **2003**, *126*, 426.
- [71] M. C. Aragoni, M. Arca, M. Caironi, C. Denotti, F. A. Devillanova, E. Grigotti, F. Isaia, F. Laschi, V. Lippolis, D. Natali, L. Pala, M. Sampietro, P. Zanello, *Chem. Comm.* **2004**, *16*, 1882.
- [72] T. Morimune, H. Kajii, Y. Ohmori, *IEEE Photonic. Tech. Lett.* **2006**, *18*, 2662.
- [73] P. Polishuk, *IEEE Commun. Mag.* **2006**, *44*, 140.
- [74] A. Pais, A. Banerjee, D. Klotzkin, I. Papautsky, *Lab on a Chip* **2008**, *8*.
- [75] F.-C. Chen, S.-C. Chien, G.-L. Cious, *Appl. Phys. Lett.* **2010**, *97*, 103301.
- [76] T. Agostinelli, M. Caironi, D. Natali, M. Sampietro, G. Dassa, E. V. Canesi, C. Bertarelli, G. Zerbi, J. Cabanillas-Gonzalez, S. De Silvestri, G. Lanzani, *J. Appl. Phys.* **2008**, *104*, 114508.
- [77] E. Perzon, X. Wang, S. Admassie, O. Inganäs, M. R. Andersson, *Polymer* **2006**, *47*, 4261.
- [78] M. M. Wienk, M. P. Struijk, R. A. J. Janssen, *Chem. Phys. Lett.* **2006**, *422*, 488.
- [79] J. B. Wang, W. L. Li, B. Chu, C. S. Lee, Z. S. Su, G. Zhang, S. H. Wu, F. Yan, *Org. Electron.* **2011**, *12*, 34.
- [80] I. H. Campbell, B. K. Crone, *Appl. Phys. Lett.* **2009**, *95*, 263302.
- [81] M. Binda, T. Agostinelli, M. Caironi, D. Natali, M. Sampietro, L. Beverina, R. Ruffo, F. Silvestri, *Org. Electron.* **2009**, *10*, 1314.
- [82] M. Binda, A. Iacchetti, D. Natali, L. Beverina, M. Sassi, M. Sampietro, *Appl. Phys. Lett.* **2011**, *98*, 073303.
- [83] B. Garreau-de Bonneval, K. I. Moineau-Chane Ching, F. Alary, T. T. Bui, L. Valade, *Coord. Chem. Rev.* **2010**, *254*, 1457.
- [84] M. C. Aragoni, M. Arca, F. A. Devillanova, F. Isaia, V. Lippolis, A. Mancini, L. Pala, G. Verani, T. Agostinelli, M. Caironi, D. Natali, M. Sampietro, *Inorg. Chem. Commun.* **2007**, *10*, 191.
- [85] M. C. Aragoni, M. Arca, M. Caironi, C. Denotti, F. A. Devillanova, E. Grigotti, F. Isaia, F. Laschi, V. Lippolis, D. Natali, L. Pala, M. Sampietro, P. Zanello, *Chem. Commun.* **2004**, *10*, 1882.
- [86] T. Agostinelli, M. Caironi, D. Natali, M. Sampietro, M. Arca, F. A. Devillanova, V. Ferrero, *Synth. Met.* **2007**, *157*, 984.
- [87] S. Dalgleish, M. M. Matsushita, L. Hu, B. Li, H. Yoshikawa, K. Awaga, *J. Am. Chem. Soc.* **2012**, *134*, 12742.
- [88] L. Beverina, R. Ruffo, M. M. Salamone, E. Ronchi, M. Binda, D. Natali, M. Sampietro, *J. Mater. Chem.* **2012**, *22*, 6704.
- [89] Y. Zhang, "Problems in the fusion of commercial high-resolution satellite images as well as Landsat 7 images and Initial solutions", presented at *ISPRS, CIG, SDH Joint International Symposium on "GeoSpatial Theory, Processing and Applications"*, Ottawa, Canada, July 8–12, **2002**.
- [90] M. de Michele, S. Leprince, J. Thiébot, D. Raucoules, R. Binet, *Remote sensing of environment* **2012**, *119*, 266.
- [91] Y. Yao, Y. Liang, V. Shrotriya, S. Xiao, L. Yu, Y. Yang, *Adv. Mater.* **2007**, *19*, 3979.
- [92] X. Gong, M. Tong, Y. Xia, W. Cai, J. S. Moon, Y. Cao, G. Yu, C.-L. Shieh, B. Nilsson, A. J. Heeger, *Science* **2009**, *325*, 1665.
- [93] C. Soci, I. W. Hwang, D. Moses, Z. Zhu, D. Waller, R. Gaudiana, C. J. Brabec, A. J. Heeger, *Adv. Funct. Mater.* **2007**, *17*, 632.
- [94] J. Peet, J. Y. Kim, N. E. Coates, W. L. Ma, D. Moses, A. J. Heeger, G. C. Bazan, *Nat. Mater.* **2007**, *6*, 497.
- [95] J. D. Zimmerman, V. V. Diev, K. Hanson, R. R. Lunt, E. K. Yu, M. E. Thompson, S. R. Forrest, *Adv. Mater.* **2010**, *22*, 2780.
- [96] J. D. Zimmerman, E. K. Yu, V. V. Diev, K. Hanson, M. E. Thompson, S. R. Forrest, *Org. Electron.* **2011**, *12*, 869.
- [97] M. S. Arnold, J. D. Zimmerman, C. K. Renshaw, X. Xu, R. R. Lunt, C. M. Austin, S. R. Forrest, *Nano Lett.* **2009**, *9*, 3354.
- [98] S. H. Im, J. A. Chang, S. W. Kim, S.-W. Kim, S. I. Seok, *Org. Electron.* **2010**, *11*, 696.
- [99] N. Cho, K. Roy Choudhury, R. B. Thapa, Y. Sahoo, T. Ohulchansky, A. N. Cartwright, K. S. Lee, P. N. Prasad, *Adv. Mater.* **2007**, *19*, 232.
- [100] G. Konstantatos, I. Howard, A. Fischer, S. Hoogland, J. Clifford, E. Klem, L. Levina, E. H. Sargent, *Nature* **2006**, *442*, 180.
- [101] D.-J. Xue, J.-J. Wang, Y.-Q. Wang, S. Xin, Y.-G. Guo, L.-J. Wan, *Adv. Mater.* **2011**, *23*, 3704.
- [102] E. Ruiz-Hitzky, M. Darder, F. M. Fernandes, E. Zatile, F. J. Palomares, P. Aranda, *Adv. Mater.* **2011**, *23*, 5250.
- [103] T. P. Osedach, N. Zhao, S. M. Geyer, L.-Y. Chang, D. D. Wanger, A. C. Arango, M. C. Bawendi, V. Bulović, *Adv. Mater.* **2010**, *22*, 5250.
- [104] T. Rauch, M. Boberl, S. F. Tedde, J. Furst, M. V. Kovalenko, G. Hesser, U. Lemmer, W. Heiss, O. Hayden, *Nat. Photon.* **2009**, *3*, 332.
- [105] D. Jarzab, K. Szendrei, M. Yarema, S. Pichler, W. Heiss, M. A. Loi, *Adv. Funct. Mater.* **2011**, *21*, 1988.
- [106] D. Ghezzi, M. R. Antognazza, M. Dal Maschio, E. Lanzarini, F. Benfenati, G. Lanzani, *Nat. Commun.* **2011**, *2*, 166.
- [107] M. R. Antognazza, D. Musitelli, S. Perissinotto, G. Lanzani, *Org. Electron.* **2010**, *11*, 357.
- [108] M. R. Antognazza, U. Scherf, P. Monti, G. Lanzani, *Appl. Phys. Lett.* **2007**, *90*, 163509.
- [109] W. A. Shapiro, *J. Opt. Soc. Am.* **1966**, *56*, 795.
- [110] H. Seo, S. Aihara, T. Watabe, H. Ohtake, M. Kubota, N. Egami, *Jpn. J. Appl. Phys.* **2007**, *46*, L1240.
- [111] Y. Higashi, K.-S. Kim, H.-G. Jeon, M. Ichikawa, *J. Appl. Phys.* **2010**, *108*, 034502.
- [112] R. N. Marks, J. J. M. Halls, D. D. C. Bradley, R. H. Friend, A. B. Holmes, *J. Phys.: Condens. Matter* **1994**, *6*, 1379.
- [113] A. K. Ghosh, T. Feng, *J. Appl. Phys.* **1978**, *49*, 5982.
- [114] K. H. An, B. O'Connor, K. P. Pipe, M. Shtein, *Org. Electron.* **2009**, *10*, 1152.
- [115] V. Gautam, M. Bag, K. S. Narayan, *J. Am. Chem. Soc.* **2011**, *133*, 17942.
- [116] E. Monroy, F. Omnes, F. Calle, *Semicond. Sci. Technol.* **2003**, *18*, R33.
- [117] M. Razeghi, A. Rogalski, *J. Appl. Phys.* **1996**, *79*, 7433.
- [118] P. Sandvik, D. Brown, J. Fedison, K. Matocha, J. Kretchmer, *J. Electrochem. Soc.* **2005**, *152*, G199.
- [119] M. Liao, Y. Koide, J. Alvarez, *Appl. Phys. Lett.* **2006**, *88*, 033504.
- [120] J. C. Carrano, T. Li, P. A. Grudowski, C. J. Eiting, R. D. Dupuis, J. C. Campbell, *Electron. Lett.* **1997**, *33*, 1980.
- [121] H. W. Lin, S. Y. Ku, H. C. Su, C. W. Huang, Y. T. Lin, K. T. Wong, C. C. Wu, *Adv. Mater.* **2005**, *17*, 2489.
- [122] Y.-Y. Lin, C.-W. Chen, W.-C. Yen, W.-F. Su, C.-H. Ku, J.-J. Wu, *Appl. Phys. Lett.* **2008**, *92*, 233301.
- [123] Q. Dai, X. Q. Zhang, *Opt. Express* **2010**, *18*, 11821.
- [124] S.-H. Wu, W.-L. Li, B. Chu, C. S. Lee, Z.-S. Su, J.-B. Wang, F. Yan, G. Zhang, Z.-Z. Hu, Z.-Q. Zhang, *Appl. Phys. Lett.* **2010**, *96*, 093302.
- [125] H.-G. Li, G. Wu, H.-Z. Chen, M. Wang, *Org. Electron.* **2011**, *12*, 70.
- [126] S.-H. Wu, W.-L. Li, B. Chu, C. S. Lee, Z.-S. Su, J.-B. Wang, Q.-J. Ren, Z.-Z. Hu, Z.-Q. Zhang, *Appl. Phys. Lett.* **2010**, *97*, 023306.
- [127] S.-H. Wu, W.-L. Li, B. Chu, Z.-S. Su, F. Zhang, C. S. Lee, *Appl. Phys. Lett.* **2011**, *99*, 023305.
- [128] J. B. Wang, W. L. Li, B. Chu, L. L. Chen, G. Zhang, Z. S. Su, Y. R. Chen, D. F. Yang, J. Z. Zhu, S. H. Wu, F. Yan, H. H. Liu, C. S. Lee, *Org. Electron.* **2010**, *11*, 1301.
- [129] G. Zhang, W. Li, B. Chu, Z. Su, D. Yang, F. Yan, Y. Chen, D. Zhang, L. Han, J. Wang, H. Liu, G. Che, Z. Zhang, Z. Hu, *Org. Electron.* **2009**, *10*, 352.
- [130] F. Yan, H. Liu, W. Li, B. Chu, Z. Su, G. Zhang, Y. Chen, J. Zhu, D. Yang, J. Wang, *Appl. Phys. Lett.* **2009**, *95*, 253308.
- [131] Y. Shiota, Y. Kuwabara, H. Inada, T. Wakimoto, H. Nakada, Y. Yonemoto, S. Kawami, K. Imai, *Appl. Phys. Lett.* **1994**, *65*, 807.

- [132] Z. Su, W. Li, B. Chu, T. Li, J. Zhu, G. Zhang, F. Yan, X. Li, Y. Chen, C.-S. Lee, *Appl. Phys. Lett.* **2008**, *93*, 103309.
- [133] C. Giebel, H. Antoniadis, D. D. C. Bradley, Y. Shirota, *Appl. Phys. Lett.* **1998**, *72*, 2448.
- [134] J. Li, C.-S. Lee, S. Lee, *J. Mater. Chem.* **2005**, *15*, 3268.
- [135] D. Ray, K. L. Narasimhan, *Appl. Phys. Lett.* **2007**, *91*, 093516.
- [136] Y. Cui, L. Liu, C. Liu, Q. Wang, W. Li, G. Che, C. Xu, M. Liu, *Synth. Met.* **2010**, *160*, 373.
- [137] P. Bhattacharya, in *Semiconductor Optoelectronic Devices*, Prentice-Hall, Upper Saddle River, NJ **1997**, 345.
- [138] D. Natali, M. Cairoli, *Adv. Mater.* **2012**, *24*, 1357.
- [139] S. Braun, W. R. Salaneck, M. Fahlman, *Adv. Mater.* **2009**, *21*, 1450.
- [140] T. Agostinelli, M. Campoy-Quiles, J. C. Blakesley, R. Speller, D. D. C. Bradley, J. Nelson, *Appl. Phys. Lett.* **2008**, *93*, 203305.
- [141] E. S. Zaus, S. Tedde, J. Furst, D. Henseler, G. H. Dohler, *J. Appl. Phys.* **2007**, *101*, 044501.
- [142] J. Xue, S. R. Forrest, *J. Appl. Phys.* **2004**, *95*, 1859.
- [143] S. Valouch, C. Hönes, S. W. Kettilitz, N. Christ, H. Do, M. F. G. Klein, H. Kalt, A. Colsmann, U. Lemmer, *Org. Electron.* **2012**, *13*, 2727.
- [144] G. Sarasqueta, K. R. Choudhury, J. Subbiah, F. So, *Adv. Funct. Mater.* **2011**, *21*, 167.
- [145] S. Dutta, K. S. Narayan, *Adv. Mater.* **2004**, *16*, 2151.
- [146] M. C. Hamilton, S. Martin, J. Kanicki, *IEEE Trans. Electron Dev.* **2004**, *51*, 877.
- [147] K. S. Narayan, N. Kumar, *Appl. Phys. Lett.* **2001**, *79*, 1891.
- [148] T. P. I. Saragi, R. Pudzich, T. Fuhrmann, J. Salbeck, *Appl. Phys. Lett.* **2004**, *84*, 2334.
- [149] Y.-Y. Noh, D.-Y. Kim, Y. Yoshida, K. Yase, B.-J. Jung, E. Lim, H.-K. Shim, *Appl. Phys. Lett.* **2005**, *86*, 043501.
- [150] Y.-Y. Noh, D.-Y. Kim, K. Yase, *J. Appl. Phys.* **2005**, *98*, 074505.
- [151] J.-M. Choi, J. Lee, D. K. Hwang, J. H. Kim, S. Im, E. Kim, *Appl. Phys. Lett.* **2006**, *88*, 043508.
- [152] Y. Guo, C. Du, C.-A. Di, J. Zheng, X. Sun, Y. Wen, L. Zhang, W. Wu, G. Yu, Y. Liu, *Appl. Phys. Lett.* **2009**, *94*, 143303.
- [153] B. Mukherjee, M. Mukherjee, Y. Choi, S. Pyo, *J. Phys. Chem. C* **2009**, *113*, 18870.
- [154] B. Mukherjee, M. Mukherjee, Y. Choi, S. Pyo, *ACS Appl. Mater. Int.* **2010**, *2*, 1614.
- [155] T. P. I. Saragi, J. Londenbergh, J. Salbeck, *J. Appl. Phys.* **2007**, *102*, 046104.
- [156] T. P. I. Saragi, R. Pudzich, T. Fuhrmann, J. Salbeck, *Appl. Phys. Lett.* **2004**, *84*, 2334.
- [157] T. P. I. Saragi, R. Pudzich, T. Fuhrmann-Lieker, J. Salbeck, *Opt. Mater.* **2007**, *29*, 879.
- [158] M. Y. Cho, S. J. Kim, Y. D. Han, D. H. Park, K. H. Kim, D. H. Choi, J. Joo, *Adv. Funct. Mater.* **2008**, *18*, 2905.
- [159] T. P. I. Saragi, M. Fettner, J. Salbeck, *Appl. Phys. Lett.* **2007**, *90*, 253506.
- [160] T. P. I. Saragi, K. Onken, I. Suske, T. Fuhrmann-Lieker, J. Salbeck, *Opt. Mater.* **2007**, *29*, 1332.
- [161] Y.-H. Kim, J.-I. Han, M.-K. Han, J. E. Anthony, J. Park, S. K. Park, *Org. Electron.* **2010**, *11*, 1529.
- [162] J. G. Labram, P. H. Wöbkenberg, D. D. C. Bradley, T. D. Anthopoulos, *Org. Electron.* **2010**, *11*, 1250.
- [163] R. Li, W. Hu, Y. Liu, D. Zhu, *Acc. Chem. Res.* **2010**, *43*, 529.
- [164] Q. Tang, L. Li, Y. Song, Y. Liu, H. Li, W. Xu, W. Hu, D. Zhu, *Adv. Mater.* **2007**, *19*, 2624.
- [165] Y. Guo, C. Du, G. Yu, C.-a. Di, S. Jiang, H. Xi, J. Zheng, S. Yan, C. Yu, W. Hu, Y. Liu, *Adv. Funct. Mater.* **2010**, *20*, 1019.
- [166] M. Y. Cho, S. J. Kim, Y. D. Han, D. H. Park, K. H. Kim, D. H. Choi, J. Joo, *Adv. Funct. Mater.* **2008**, *18*, 2905.
- [167] M. Mas-Torrent, P. Hadley, N. Crivillers, J. Veciana, C. Rovira, *Chem. Phys. Chem.* **2006**, *7*, 86.
- [168] K. H. Kim, S. Y. Bae, Y. S. Kim, J. A. Hur, M. H. Hoang, T. W. Lee, M. J. Cho, Y. Kim, M. Kim, J.-I. Jin, S.-J. Kim, K. Lee, S. J. Lee, D. H. Choi, *Adv. Mater.* **2011**, *23*, 3095.
- [169] K. S. Narayan, N. Kumar, *Appl. Phys. Lett.* **2001**, *79*, 1891.
- [170] S. Dutta, K. S. Narayan, *Phys. Rev. B* **2003**, *68*, 125208.
- [171] H. J. Queisser, *Phys. Rev. Lett.* **1985**, *54*, 234.
- [172] M. C. Hamilton, J. Kanicki, *IEEE J. Sel. Top. Quant.* **2004**, *10*, 840.
- [173] M. C. Hamilton, S. Martin, J. Kanicki, *IEEE T. Electron Dev.* **2004**, *51*, 877.
- [174] X. Wang, K. Wasapinyokul, W. D. Tan, R. Rawcliffe, A. J. Campbell, D. D. C. Bradley, *J. Appl. Phys.* **2010**, *107*, 024509.
- [175] Y. Xu, P. R. Berger, J. N. Wilson, U. H. F. Bunz, *Appl. Phys. Lett.* **2004**, *85*, 4219.
- [176] H. Dong, H. Li, E. Wang, H. Nakashima, K. Torimitsu, W. Hu, *J. Phys. Chem. C* **2008**, *112*, 19690.
- [177] K. Wasapinyokul, W. I. Milne, D. P. Chu, *J. Appl. Phys.* **2009**, *105*, 024509.
- [178] T. D. Anthopoulos, *Appl. Phys. Lett.* **2007**, *91*, 113513.
- [179] S. M. Mok, F. Yan, H. L. W. Chan, *Appl. Phys. Lett.* **2008**, *93*, 023310.
- [180] F. Yan, J. Li, S. M. Mok, *J. Appl. Phys.* **2009**, *106*, 074501.
- [181] R. M. Meixner, H. Gobel, F. A. Yildirim, W. Bauhofer, W. Krautschneider, *Appl. Phys. Lett.* **2006**, *89*, 092110.
- [182] E. Kraker, A. Haase, B. Lamprecht, G. Jakopic, C. Konrad, S. Kostler, *Appl. Phys. Lett.* **2008**, *92*, 033302.
- [183] B. Lamprecht, H. Ditlbacher, G. Jakopic, J. R. Krenn, *physica status solidi (RRL)–Rapid Research Letters* **2008**, *2*, 266.
- [184] Y. Ohmori, H. Kajii, M. Kaneko, K. Yoshino, M. Ozaki, A. Fujii, M. Hikita, H. Takenaka, T. Taneda, *IEEE J. Sel. Top. Quant.* **2004**, *10*, 70.
- [185] M. Punke, S. Valouch, S. W. Kettilitz, M. Gerken, U. Lemmer, *J. Lightwave Technol.* **2008**, *26*, 816.
- [186] A. Weinert, *Plastic Optical Fibers*, Publicis MCD Verlag, Erlangen, Germany **1999**.
- [187] M. Binda, C. Rottundi, A. Iacchetti, D. Natali, M. Sampietro, L. Beverina, “Organic photodetector directly deposited onto the cut end of a plastic optical fiber”, presented at *2012 Symposium on Photonics and Optoelectronics (SOPO)*, Shanghai, **2012**.
- [188] X. Xu, M. Davanco, X. Qi, S. R. Forrest, *Org. Electron.* **2008**, *9*, 1122.
- [189] C. K. Renshaw, X. Xu, S. R. Forrest, *Org. Electron.* **2010**, *11*, 175.
- [190] X. Tong, S. R. Forrest, *Org. Electron.* **2011**, *12*, 1822.
- [191] S. W. Jeong, J. W. Jeong, S. Chang, S. Y. Kang, K. I. Cho, B. K. Ju, *Appl. Phys. Lett.* **2010**, *97*, 253309.
- [192] S. Aihara, H. Seo, M. Namba, T. Watabe, H. Ohtake, M. Kubota, N. Egami, T. Hiramatsu, T. Matsuda, M. Furuta, H. Nitta, T. Hirao, *IEEE T. Electron Dev.* **2009**, *56*, 2570.
- [193] S. Tedde, E. S. Zaus, J. Furst, D. Henseler, P. Lugli, *IEEE T. Electron Dev.* **2007**, *28*, 893.
- [194] D. Baierl, L. Pancheri, M. Schmidt, D. Stoppa, G.-F. Dalla Betta, G. Scarpa, P. Lugli, *Nat. Commun.* **2012**, *3*, 1175.
- [195] I. Nausieda, K. Ryu, I. Kymissis, A. I. Akinwande, V. Bulovic, C. G. Sodini, *IEEE T. Electron Dev.* **2008**, *55*, 527.
- [196] B. P. Rand, J. Xue, M. Lange, S. R. Forrest, *IEEE Photonic. Tech. Lett.*, **2003**, *15*, 1279.
- [197] J. Cabanillas-Gonzalez, O. Pena-Rodriguez, I. S. Lopez, M. Schmidt, M. I. Alonso, A. R. Goni, M. Campoy-Quiles, *Appl. Phys. Lett.* **2011**, *99*, 103305.
- [198] L. L. Lavery, G. L. Whiting, A. C. Arias, *Org. Electron.* **2011**, *12*, 682.
- [199] Y. Guo, G. Yu, Y. Liu, *Adv. Mater.* **2010**, *22*, 4427.
- [200] J. Lee, P. Jadhav, M. A. Baldo, *Appl. Phys. Lett.* **2009**, *95*, 033301.
- [201] W.-W. Tsai, Y.-C. Chao, E.-C. Chen, H.-W. Zan, H.-F. Meng, C.-S. Hsu, *Appl. Phys. Lett.* **2009**, *95*, 213308.

- [202] D. Baierl, B. Fabel, P. Gabos, L. Pancheri, P. Lugli, G. Scarpa, *Org. Electron.* **2010**, *11*, 1199.
- [203] T. P. OSEDACH, S. M. GEYER, J. C. HO, A. C. ARANGO, M. G. BAWENDI, V. BULOVIC, *Appl. Phys. Lett.* **2009**, *94*, 043307.
- [204] Z. Kong, W. Li, G. Che, B. Chu, D. Bi, L. Han, L. Chen, Z. Hu, Z. Zhang, *Appl. Phys. Lett.* **2006**, *89*, 161112.
- [205] G. Zhang, W. Li, B. Chu, F. Yan, J. Zhu, Y. Chen, *Appl. Phys. Lett.* **2010**, *96*, 073301.
- [206] L. L. Chen, W. L. Li, H. Z. Wei, B. Chu, B. Li, *Sol. Energy Mater. Sol. Cells* **2006**, *90*, 1788.
- [207] Z. Si, B. Li, L. Wang, S. Yue, W. Li, *Sol. Energy Mater. Sol. Cells* **2007**, *91*, 1168.
- [208] J.-E. Park, B. Mukherjee, H. Cho, S. Kim, S. Pyo, *Synth. Met.* **2011**, *161*, 143.
- [209] B. Lucas, A. El Amrani, M. Chakaroun, B. Ratier, R. Antony, A. Moliton, *Thin Solid Films* **2009**, *517*, 6280.
- [210] Y.-Y. Noh, J. Ghim, S.-J. Kang, K.-J. Baeg, D.-Y. Kim, K. Yase, *J. Appl. Phys.* **2006**, *100*, 094501.
- [211] Y. Sun Kim, S. Young Bae, K. Hwan Kim, T. Wan Lee, J. A. Hur, M. Ha Hoang, M. Ju Cho, S.-J. Kim, Y. Kim, M. Kim, K. Lee, S. Joong Lee, D. Hoon Choi, *Chem. Commun.* **2011**, *47*, 8907.
- [212] S. Dutta, K. S. Narayan, *Synth. Met.* **2004**, *146*, 321.
- [213] P. Tanusri, M. Arif, I. K. Saiful, *Nanotechnology* **2010**, *21*, 325201.